Inorganic Chemistry

pubs.acs.org/IC Article

Gold(I) and Silver(I) Complexes with 2-Anilinopyridine-Based Heterocycles as Multitarget Drugs against Colon Cancer

Inés Mármol, Sara Montanel-Perez, José Carlos Royo, M. Concepción Gimeno,* M. Dolores Villacampa, M. Jesús Rodríguez-Yoldi,* and Elena Cerrada*

Cite This: https://dx.doi.org/10.1021/acs.inorgchem.0c02922 Read Online

ACCESS | Metrics & More | Article Recommendations | Supporting Information

ABSTRACT: A series of gold(I) and silver(I) derivatives with N- or S-donor ligands derived from 2-anilinopyridine has been synthesized and characterized. The mononuclear structure of $[Au(L1)(PPh_3)](TfO)$ (**1a**) and $[Au(L2)(PPh_3)](TfO)$ (**1b**) was confirmed by X-ray diffraction studies, as well as the dinuclear structure in the case of $[Ag(TfO)(L1)]_2$ (**4a**). Most of the complexes are cytotoxic against a model of colorectal adenocarcinoma (Caco-2 cell line) and breast adenocarcinoma cancer cell lines (MCF-7). $[Au(L1)(PPh_3)](TfO)$ (**1a**) was able to induce caspases 8 and 3 activation, loss of mitochondrial membrane potential, and reactive oxygen species (ROS)-dependent cell death on Caco-2 cells upon 24 h incubation. In addition, the gold complex **1a** produced a significant inhibition of the redox enzyme thioredoxin reductase as well as 20S proteasome. However, the silver(I) analogue, $[Ag(TfO)(L1)(PPh_3)]$ (**2a**), induced cell death independent of inhibition of thioredoxin reductase and 20S proteasome, triggered ROS-independent apoptosis mediated by caspase 8 and 3 activation, and loss of mitochondrial membrane potential, which points to a different mechanism of action for both derivatives, dependent on the metal center.

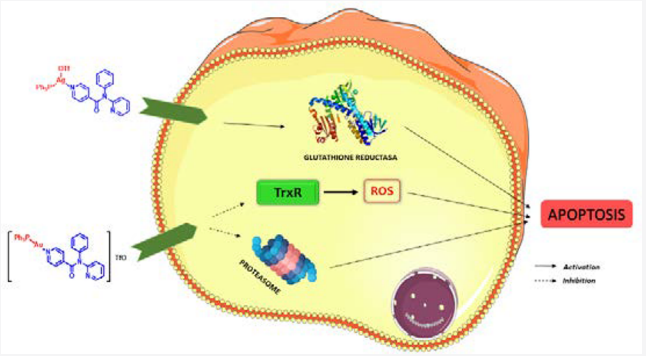

1. INTRODUCTION

The use of platinum-based anticancer drugs in chemotherapy is accompanied by the presence of side effects such as gastrointestinal and hematological toxicity in addition to drug-resistance phenomena.[1,2] In order to circumvent these drawbacks new metallodrugs have been designed on the basis of non-platinum metals, such as ruthenium or gold.

Gold complexes interact with cellular proteins[3−5] instead of DNA, the main target of the platinum-based complexes, which suppose an important advantage in order to overcome the limitations found in platinum derivatives. Consequently, gold compounds are an interesting alternative to platinum-based drugs. Thus, a huge amount of gold derivatives, mainly gold(I) complexes, has been tested against different types of cancer cells.[6−14] In addition to gold, other metals such as silver are emerging as potential anticancer agents.[15−23]

Silver complexes have been used as antimicrobial agents for many years[24−27] mainly in the form of inorganic salts or complexes, such as silver nitrate[28] and silver sulfadiazine. The latter is a sulfonamide-based derivative introduced in 1968[29] and is used as one of the most effective topical burn treatments,[30] thanks to its antibacterial properties.[31] Although silver is not an endogenous element, its toxicity in humans seems to be quite low. The body can tolerate the presence of silver in low doses without any toxic effects;[32] consequently this low toxicity constitutes one of the greatest advantages of silver derivatives over other metallodrugs.

The mechanism of the anticancer activity of the silver derivatives is not well established; however, several possible targets have been identified. Thus, some examples have exerted antiproliferative effects by inhibition of the activity of the redox enzyme thioredoxin reductase (TrxR),[33] by noncovalent interaction with DNA[34] (interactions as $\pi-\pi$ stacking contacts),[35] by topoisomerase I inhibition[36] or by LOX (lipoxygenase) inhibition activity.[34] In general, silver complexes induce cell death via apoptosis and depolarization of the mitochondrial membrane potential ($\Delta\psi$).[37]

Although the mechanism of action of silver derivatives has not been fully clarified, it involves the release of the silver ion inside the cell that disrupts its function.[38] Consequently the choice of the ligands that can strongly coordinate the metallic center and facilitate the slow release of Ag^+ is essential. With this idea, a significant amount of silver complexes with a great

Received: October 5, 2020

https://dx.doi.org/10.1021/acs.inorgchem.0c02922
Inorg. Chem. XXXX, XXX, XXX−XXX

Scheme 1. (i) [M(TfO)(PPh_3)] (M = Au, 1a,b; M = Ag, 2a,b); (ii) 2 [Ag(TfO)(PPh_3)]; (iii) AgTfO; (iv) (1/2)AgTfO

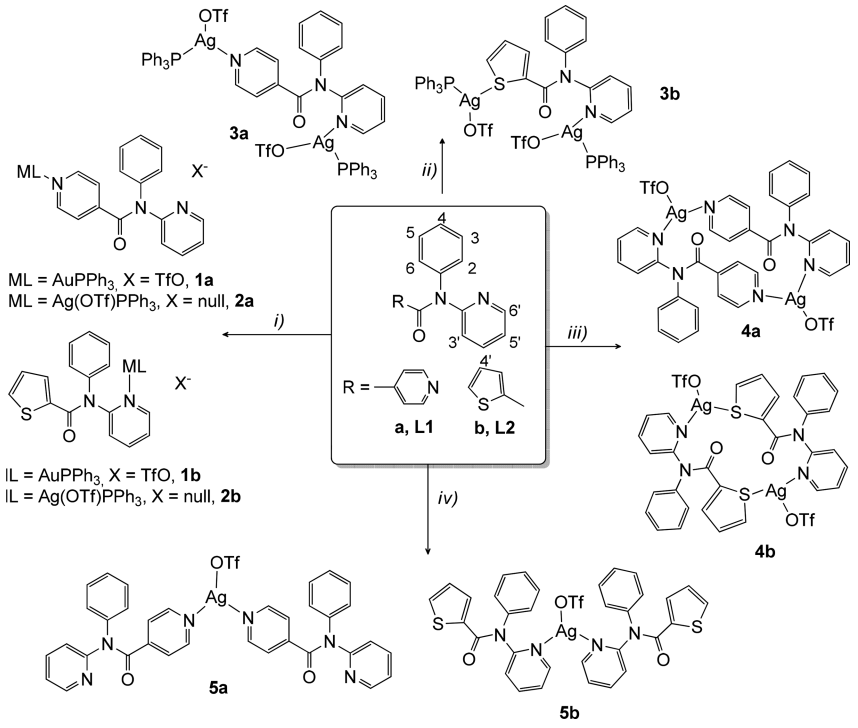

variety of ligands has been designed for potential pharmaceutical usage.[16,18,19,21] Thus, silver N-heterocyclic carbene (NHC) complexes[15,17,22−24,39] constitute the group with the largest number of examples of Ag(I) compounds with biological properties, mainly due to their strong coordination to the metallic center and their increased stability. Apart from Ag-NHC derivatives, silver coordination compounds with a high number of different ligands (carboxylic acids ligands;[40] phosphines;[41,42] amino acids ligands;[43] N-donor ligands;[44,45] S-donor ligands;[46] and mixed ligands, such as N,O-,[47,48] N,S-,[49] and P,O-donor ligands[50]) have been recently described as potential anticancer silver-based complexes.

With this background, we describe here the synthesis of new heterocyclic N- and N,S-donor ligands derived from 2-anilinopyridine containing also thiophene or pyridine moieties. The choice of the anilino moiety is based on the properties exhibited by heterocyclic systems and molecules on the basis of this unit.[51,52] Furthermore, the easy functionalization with pyridine of thiophene, the latter a five aromatic sulfur-containing heterocycle encountered in many therapeutically active agents, may confer to these ligands interesting biological properties.[53,54] Additionally, coordination to silver and gold metallic centers may enhance those properties. New mononuclear silver derivatives, their gold analogs, and dinuclear Ag(I) complexes have been described and their biological activity evaluated against Caco-2 and MCF-7 cancer cells. Redox enzymes thioredoxin reductase and glutathione reductase (GR) as well as 20S proteasome have been investigated as likely targets of selected gold(I) and silver(I) complexes. Moreover, measurement of reactive oxygen species (ROS) and cell death studies have been performed.

2. RESULTS AND DISCUSSION

2.1. Synthesis of Ligands and Complexes. The reaction of 2-anilinopyridine with 4-chlorocarbonylpyridine or 2-chlorocarbonylthiophene in the presence of NEt_3, in order to neutralize the HCl generated, affords the corresponding ligands L1 (R = 4-pyridine) and L2 (R = 2-thiophene) after amide bond formation (Scheme 1).

The addition of both ligands to a freshly prepared solution of [Au(TfO)(PPh_3)] or to a solution of [Ag(TfO)(PPh_3)] leads to the formation of the phosphane gold(I) complexes [AuL(PPh_3)]TfO (L = L1, **1a**; L2, **1b**) and the phosphane silver(I) derivatives [Ag(TfO)L(PPh_3)] (L = L1, **2a**; L2, **2b**, Scheme 1).

The asymmetric sulfonyl stretching frequencies characteristic of ionic triflate group[55] are observed in the IR spectra of both gold complexes (**1a**,**b**), which is corroborated in their $^{19}F\{^1H\}$ NMR with a singlet centered at −80 ppm. However, silver derivatives (**2a**,**b**) exhibit a downfield signal in their $^{19}F\{^1H\}$ NMR spectra at around −78 ppm, characteristic of a coordinated triflate ligand and the absence of the band in the region of 1260 cm^{-1}, attributed to ionic TfO in their IR spectra.

A downfield displacement of the pyridine resonances next to the carbonyl moiety is observed in the ^1H NMR spectra of complexes **1a** and **2a**, which is in accordance with the coordination of the $AuPPh_3$ moiety through the N atom of that pyridine. Ligand L2 has replaced such pyridine by a thiophene unit, which signals remain unchanged after gold coordination in complexes **1b** and **2b**. Instead, the resonances of the pyridine molecule of the amine are shifted downfield, due to the coordination of the metallic center through its N atom.

The $^{31}P\{^1H\}$ NMR spectra of the gold derivatives display a singlet centered at around 30 ppm, which points to the presence of a unique $AuPPh_3$ fragment. In the case of silver complexes, their $^{31}P\{^1H\}$ NMR spectra show a broad signal at room temperature that splits into two doublets at 200 K, due to the coupling of the phosphorus atom with silver isotopomers (^{109}Ag and ^{107}Ag).

https://dx.doi.org/10.1021/acs.inorgchem.0c02922
Inorg. Chem. XXXX, XXX, XXX−XXX

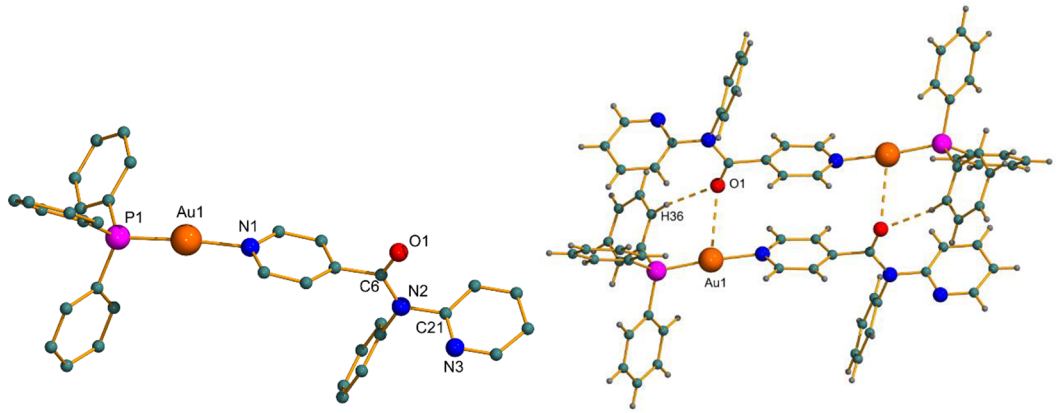

Figure 1. (A) Molecular structure of the cation of complex **1a**. Hydrogens have been omitted for clarity. (B) View of the intramolecular interactions in complex **1a**.

The addition of 2 equiv of $[Ag(TfO)(PPh_3)]$ to ligands L1 and L2 leads to the preparation of the dinuclear phosphane silver(I) derivatives **3a** and **3b** (Scheme 1). The NMR data of these complexes are in accordance with the coordination of two $AgPPh_3$ fragments to both pyridine units in **3a** and to the pyridine and thiophene molecules in **3b**. Likewise, the occurrence of two sets of two doublets in the $^{31}P\{^1H\}$ NMR spectra at 200 K in **3b** is in agreement with two different phosphorus environments as a consequence of the coordination of the $AgPPh_3$ fragments to the pyridine and thiophene rings through the N and S atoms, respectively. However, only two doublets are observed in **3a**, pointing to a similar coordination environment since two pyridine rings are coordinated to the $AgPPh_3$ units. In addition, complex **3a** displays two sets of doublets with lower intensity, centered at 10.9 ppm, that correspond to the $[Ag(PPh_3)_2]^+$ moiety, which appears in solution along the time.

The reaction of AgTfO with L1 or L2 in 1:1 and 1:2 molar ratios affords the dinuclear $[Ag_2(TfO)_2L_2]$ (L = L1, **4a**; L2, **4b**) and the mononuclear $[Ag(TfO)L_2]$ (L = L1, **5a**; L2, **5b**) derivatives, respectively (Scheme 1). Coordination of the AgTfO fragment to both pyridine molecules in **4a** and to pyridine and thiophene units in **4b** is evidenced by the corresponding NMR downfield displacements and by X-ray analysis in the case of **4a**. On the other hand, ^1H NMR of complex **5a** displays solely displacements in the acylpyridine resonances and **5b** in the pyridine ring of the amine, in accordance with the proposed structure depicted in Scheme 1.

All of the complexes have been completely characterized by NMR studies, IR spectroscopy, elemental analysis, and mass spectrometry, and in the particular cases of L1, L2, **1a**, **1b**, and **4a**, additional X-ray analysis corroborated the proposed structures. The experimental data point to a monodentate coordination of the ligands to the metallic centers of gold or silver through the N atom of the ligands, except in the cases of the dinuclear derivatives **3b** and **4b**, where additional coordination to the S atom of ligand L2 justify the dinuclear structure.

2.2. X-ray Diffraction Analyses. Molecular structures of L1 and L2 and complexes **1a**, **1b**, and **4a** have been confirmed by X-ray crystallographic studies. L1 and L2 crystallize in the monoclinic space group $P2_1/c$ with one molecule by asymmetric unit. The molecular structures are shown in Figure S1 (Supporting Information) and confirm the nature of the compounds. The bond lengths and angles within them are as expected.

The structure of complex **1a** is shown in Figure 1A. The coordination of the $AuPPh_3$ fragment takes place with the N atom of the acylpyridine group, with Au−N and Au−P bond distances of 2.077(5) Å and Au1−P1 2.2371(16) Å, respectively. The geometry around the gold center is slightly distorted from linearity with a P−Au−N angle of 174.46(15)°. The molecules are associated in the lattice due to the presence of intermolecular interactions of the gold center with the oxygen atom of the carbonyl group, Au1···O1 3.003 Å, in addition to hydrogen-bonding interactions with one of the phenyl groups of the PPh_3 ligand, with a distance acceptor−donor O1···H−C36 of 3.278 Å (Figure 1b).

The molecular structure of complex **1b** has also been established by X-ray diffraction and is shown in Figure 2. In

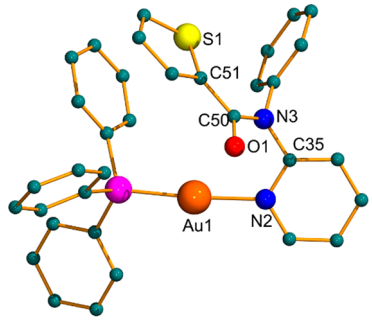

Figure 2. Molecular structure of **1b**, showing the cation. Hydrogens have been omitted for clarity.

contrast to complex **1a** the coordination of the gold atom takes place with the pyridine ring of the 2-anilinopyridine in complex **1b** and not with the sulfur atom of the thiophene, corroborating the poor nucleophilicity of this moiety. The Au−N and Au−P distances are similar to those in complex **1a**, 2.083(5) Å and 2.2398(16) Å, respectively. The geometry of the gold center is also linear, N−Au−P angle of 175.21(14)°. In this case probably because of the presence of a bulkiest sulfur atom there are not short intermolecular distances in the molecule.

https://dx.doi.org/10.1021/acs.inorgchem.0c02922
Inorg. Chem. XXXX, XXX, XXX−XXX

The structure of complex **4a** was also measured, but the data obtained, although they allow the determination of the molecular structure, are of low quality and consequently not accurate parameters can be obtained. However, the molecule shown in Figure 3 confirms the nature of the compound,

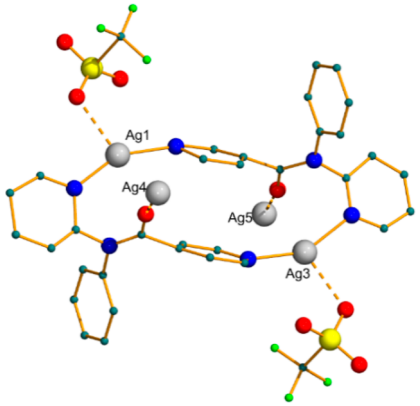

Figure 3. Molecular structure of **4a**, showing the basic dinuclear unit and the further contacts with other oxygen atoms.

presenting an interesting three-dimensional polymer, in which there are a dinuclear silver unit with the ligand bonded to the silver through both pyridine groups as bridging ligand. Additionally, the silver atoms bond the oxygen of the carbonyl group and one of the triflare anion forming the 3D network.

The stability of the free ligand and complexes was analyzed by UV−vis absorption spectroscopy in PBS solution (pH = 7.4). Solutions suitable for spectrophotometric analysis were prepared by diluting dimethyl sulfoxide (DMSO) mother solutions of the complexes with PBS buffer. The resulting solutions were monitored over 24 h at 37 °C. The spectra of the free ligands and their corresponding complexes (Figure S32) show an intense absorption band at ca. 210 nm and one lower energy absorption band with low intensity around 260 nm, which could be assigned as $\pi \rightarrow \pi^*$ intraligand transitions. These bands remain without any changes in shape or displacement in the absorbance maximum (no apparent red or blue shift) in all of the new derivatives, in addition to a lack of absorbance at around 500 nm in the case of gold compounds, over 24 h, implying a substantial stability of the chromophore under physiological conditions.

2.3. Biological Studies. *2.3.1. Antiproliferative Effect of Gold(I) and Silver(I) Complexes.* The anticancer effect of gold(I) and silver(I) complexes was evaluated on two cell lines: Caco-2, a model of colorectal adenocarcinoma, and MCF-7, an estrogen receptor-positive breast carcinoma model. Cell culture was incubated 72 h with a range of concentration of each complex, and IC_{50} values were obtained. The antiproliferative effect of both ligands was also tested, and two reference drugs—cisplatin and auranofin—were included as positive controls. All calculated IC_{50} are shown on Table 1.

Most of the evaluated complexes display higher toxicity in comparison to cisplatin in terms of IC_{50}, except complex **4a** which has no antiproliferative effect on the MCF-7 cell line. Moreover, IC_{50} of complex **1a** on both cancer models is comparable to those obtained with auranofin, suggesting that **1a** might be a promising antitumor agent.

Although both gold(I) complexes tend to show greater antiproliferative effect than each silver(I) complex analyzed, complex **3a** displayed the lowest IC_{50} value, which suggests it might be the most promising agent. However, this compound evolves to an equilibrium of species in DMSO solution, among which $[Ag(PPh_3)_2]TfO$ was identified. Therefore, the observed anticancer effect might be caused by a mix of molecules instead of a single one, and the complex was not considered on further assays.

When comparing the antiproliferative effect of series **1a**−**5a** and **1b**−**5b**, results shown in Table 1 suggest minor influence of the ligand L1 or L2 on the biological activity of the final metallodrug. However, some exceptions have been observed: complex **1a** displays higher antiproliferative effect than **1b** on MCF-7 cell line; complex **4a** has no effect on MCF-7 cells, whereas **4b** does; finally, **5b** shows greater anticancer effect toward both cell lines than its counterpart **5a**.

The free ligands displayed considerably antiproliferative effect against MCF-7 cells; however, only L2 showed moderate activity against Caco-2 cells. However, coordination to the metallic center resulted in a significant increase of the antitumor activity, which might suggest that the observed

Table 1. IC_{50} (μM) Values of Gold(I) and Silver(I) Derivatives as Well as the Free Ligands and Two Reference Drugs—Cisplatin and Auranofin—as Positive Control on Caco-2, MCF-7 and Differentiated Caco-2 Cells upon 72 h Incubation[a]

	IC_{50} (μM)			selectivity index	
compd	Caco-2	MCF-7	differentiated Caco-2 cells	Caco-2	MCF-7
L1	>100	17.45 ± 8.16	125.76 ± 13.43	1.26	7.21
$[Au(L1)(PPh_3)](TfO)$ (**1a**)	2.23 ± 0.21	0.46 ± 0.56	39.40 ± 23.39	17.67	85.65
$[Ag(TfO)(L1)(PPh_3)]$ (**2a**)	5.52 ± 1.89	7.22 ± 0.69	9.44 ± 2.12	1.71	1.31
$[Ag_2(TfO)_2(L1)(PPh_3)_2]$ (**3a**)	0.25 ± 0.10	4.10 ± 0.44	10.88 ± 2.82	43.52	2.65
$[Ag(TfO)(L1)]_2$ (**4a**)	7.50 ± 3.14	>100	48.74 ± 10.01	6.50	
$[Ag(TfO)(L1)_2]$ (**5a**)	10.22 ± 5.02	15.60 ± 1.08	120.51 ± 11.52	11.79	7.73
L2	48.54 ± 13.32	12.48 ± 5.32	124.29 ± 7.50	2.56	9.96
$[Au(L2)(PPh_3)](TfO)$ (**1b**)	3.75 ± 0.41	3.53 ± 0.52	13.53 ± 0.02	3.61	3.83
$[Ag(TfO)(L2)(PPh_3)]$ (**2b**)	7.11 ± 0.92	6.71 ± 0.01	10.23 ± 4.02	1.44	1.52
$[Ag_2(TfO)_2(L2)(PPh_3)_2]$ (**3b**)	14.41 ± 2.61	7.43 ± 0.49	39.65 ± 19.06	2.75	5.34
$[Ag(TfO)(L2)]_2$ (**4b**)	1.32 ± 0.47	2.65 ± 0.32	55.40 ± 1.43	41.97	20.91
$[Ag(TfO)(L2)_2]$ (**5b**)	4.22 ± 2.00	0.90 ± 0.11	80.26 ± 26.90	19.02	89.18
cisplatin	8.9 ± 0.76[56]	7.6 ± 2.96[57]			
auranofin	1.80 ± 0.10	0.77 ± 0.05	6.21 ± 0.44	3.45	8.06

[a]Selectivity index values are also shown. Results are expressed as mean ± SE of at least three determinations, after 72 h incubation.

https://dx.doi.org/10.1021/acs.inorgchem.0c02922
Inorg. Chem. XXXX, XXX, XXX−XXX

effect depends on both the ligand and the metal. This statement is especially relevant for **1a**−**5a** series on Caco-2, since the lack of antiproliferative effect of L1 highlights the key role of gold or silver on the biological activity of the metallodrug. We found no significant differences when comparing IC_{50} values of the free ligands and the new complexes due to the great statistical errors obtained upon IC_{50} calculation of such free ligands. These data suggest that coordination of the metallic center with the corresponding ligand results in an increase of the antitumor potential compared to the free ligand as well as in an improvement of the reproducibility.

The significant antiproliferative effect displayed by most of the tested complexes as well as the free ligands L1 and L2 on MCF-7 cell line was somehow atypical in comparison to previous results obtained by some of us when comparing the effect of selected gold(I) complexes on Caco-2 and MCF-7 cells. In our experience, gold(I) complexes usually show greater anticancer activity on our colorectal adenocarcinoma model rather than on the breast adenocarcinoma one.[58,59] Similar results have been observed by other authors.[60] In a previous work, we found that the alkynyl gold(I) complex [Au(L)PPh_3] (L = 2-(4-bromophenyl)-3-(prop-2-ynyloxy)-4*H*-chromen-4-one) was able to inhibit cycloocygenase-2 (COX-2) activity; since that isoform is not expressed on MCF-7 cells,[61] the tested complex showed higher antiproliferative effect on other cancer models that actually expressed that enzyme.[58] Given that in our present study we found the opposite effect, we hypothesized that our metallic derivatives might interact with a molecular target found on MCF-7 line but not on Caco-2. Since MCF-7 is an estrogen receptor-positive breast adenocarcinoma model, first we decided to evaluate the effect of selected complexes on an estrogen receptor-negative MDA-231 cell line to determine their effect on a different subtype of breast adenocarcinoma. As can be observed on Table 2, both gold(I) complexes studied, [Au(L1)(PPh_3)](TfO) (**1a**) and [Au(L2)(PPh_3)](TfO) (**1b**), displayed significant ($p < 0.05$) anticancer activity when compared to the free ligands L1 and L2, respectively, which suggest that the observed effect is mainly a direct consequence of coordination to the metallic center. Complex **1a** showed a similar behavior on both breast adenocarcinoma models, thus suggesting that its anticancer effect might be independent of estrogen-receptor expression. On the other hand, the IC_{50} value of **1b** was ca. 13 times higher on MCF-7 than on MDA-231 cells. Therefore, this complex might be selective for estrogen receptor-positive breast adenocarcinoma cells. It is interesting to highlight that coordination ligand L2 has no effect on MDA-231 cells; thus, it is feasible to assume that the observed effect on this cancer model is due to the presence of the gold atom.

Table 2. IC_{50} (μM) Values of Gold(I) Complexes as Well as Coordination Ligands on MDA-231 Cells upon 72 h Incubation[a]

compd	IC_{50} (μM)
L1	5.69 ± 0.11
[Au(L1)(PPh_3)](TfO) (**1a**)	0.78 ± 0.20*
L2	154.09 ± 0.01
[Au(L2)(PPh_3)](TfO) (**1b**)	0.27 ± 0.05*

[a]Results are expressed as mean ± SE of at least three determinations. (*) $p < 0.05$ vs free ligand.

In order to evaluate the effect of our complexes on a noncancerous model, we calculated IC_{50} values after 72 h incubation on differentiated Caco-2 cells, which can be used as a gastrointestinal barrier model.[62] Furthermore, we obtained selectivity index (SI) using these data and the previous IC_{50} values calculated on cancer models as previously was described by Badisa et al.[63] As is shown in Table 1, some of the evaluated complexes displayed higher SI values than the reference drug auranofin, thus suggesting that their clinical use might be safer. In addition, ligands L1 and L2 showed lower SI values than the positive controls and most of the tested complexes. Therefore, although both molecules have previously showed a certain antiproliferative effect, they must be discarded as potential anticancer agents due to their likely low selectivity.

Considering all data showed on Table 1, complexes **1a** and **2a** were selected for further assays to determine their likely mechanism of action and kind of cell death triggered upon treatment on Caco-2 cancer cells. Since the unique difference between those complexes was the presence of a gold or silver atom, this would also lead us to perform an in-depth comparison of the anticancer effect on the basis of both metallic centers.

2.3.2. Cell Death Studies. Caco-2 cells were incubated 48 h with the IC_{50} of both complexes **1a** and **2a**, and apoptotic populations were analyzed with double annexin V-FITC and propidium iodide staining by flow cytometry. According to Figure 4, neither of the analyzed complexes induced an increase in necrotic population. Instead, upon treatment with complex **1a** a 4.4-up-fold on early apoptotic population and a 7-up-fold on late apoptotic population were observed. Similarly, the silver complex **2a** triggered a 7.7-up-fold on early apoptotic cells along with a 3.6-up-fold on late apoptotic cells. Taken together, these results suggest that both gold(I) and silver(I) complexes are able to induce apoptosis on Caco-2 cells, although the gold-containing derivative seems to trigger cell death faster than the silver(I) counterpart.

Other apoptotic biomarkers were determined in order to confirm results shown on Figure 4. Since this kind of cell death usually depends on caspases activation,[64,65] we analyzed caspase 8 and executioner caspase 3 activation upon 48 h of treatment with complexes **1a** and **2a**, respectively. We found a significant increase in activation of both caspases (Figure 5A,B), which might be in accordance with the increase in apoptotic populations previously observed (Figure 4).

Caspase 8 activation suggests that the tested complexes are able to trigger extrinsic apoptosis. Most of the studies performed with regard to the anticancer activity of gold(I) derivatives have focused on their capacity to induce intrinsic apoptosis; however, some authors have reported that auranofin is also able to trigger cancer cell death via extrinsic apoptosis.[66,67] Given that extrinsic apoptosis depends on cell death receptors activation, it remains unclear the mechanism by which auranofin induces this pathway. However, since some authors have noticed that aberrant ROS levels could elicit cell death receptors activation,[68] it has been proposed that the pro-oxidant effect of this metallodrug might be responsible for caspase 8 activation as a consequence. On the other hand, no evidence have been found with regard to further silver(I) complexes able to induce caspase 8 activation to date. To our knowledge, this might be the first report of a silver-containing

https://dx.doi.org/10.1021/acs.inorgchem.0c02922
Inorg. Chem. XXXX, XXX, XXX−XXX

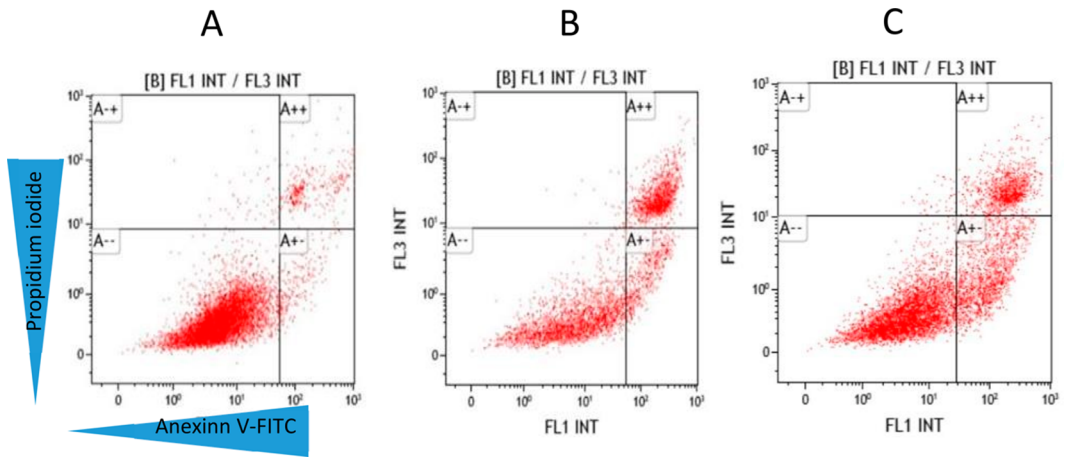

Figure 4. Analysis of the type of cell death induced on undifferentiated Caco-2 cells after 48 h incubation with (A) DMSO (negative control), (B) [Au(L1)(PPh_3)](TfO) (**1a**) (IC_{50}), and (C) [Ag(TfO)(L1)(PPh_3)] (**2a**) (IC_{50}). Percentages of alive, necrotic, early apoptotic, and late apoptotic cells are indicated.

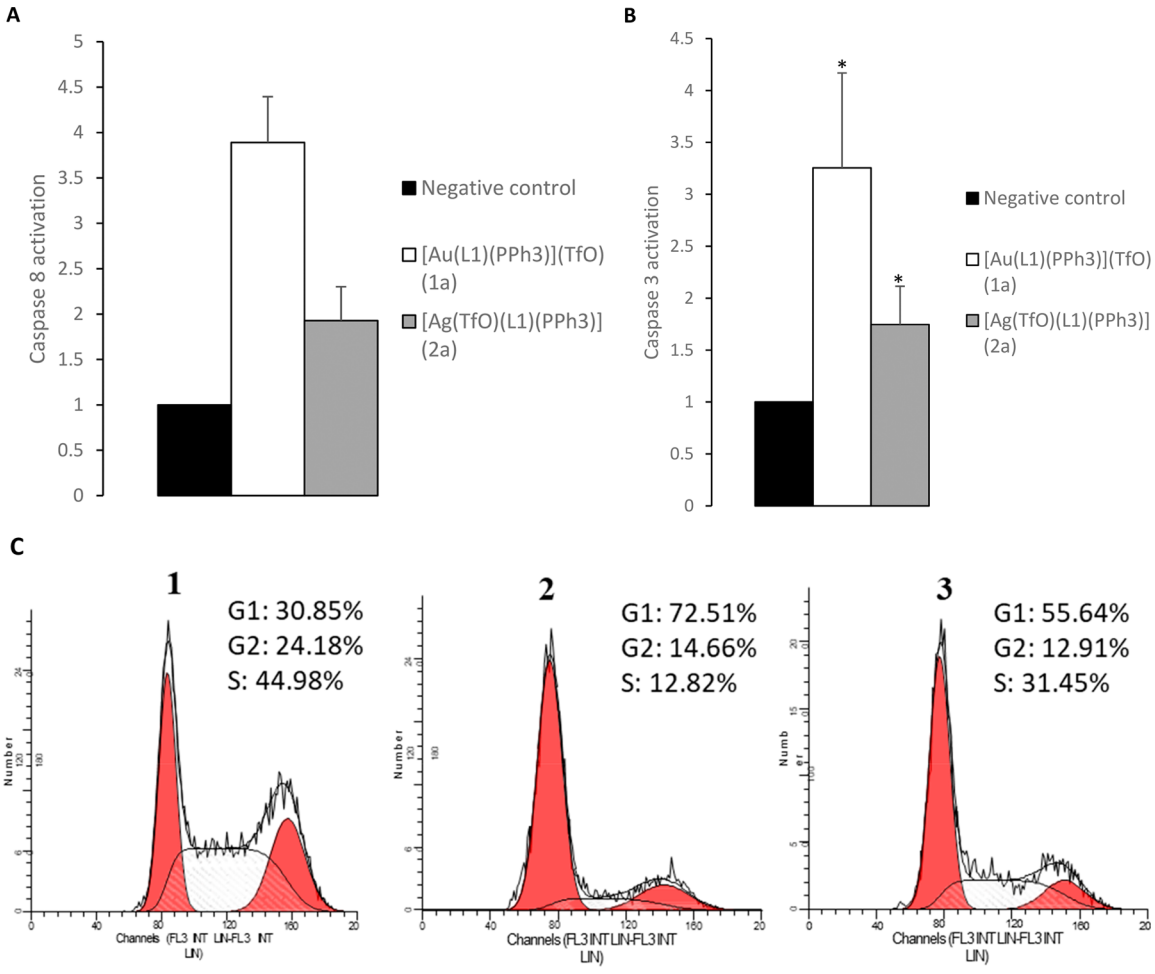

Figure 5. Analysis of apoptosis biomarkers on Caco-2 cells after 48 h incubation with complexes **1a** and **2a** (IC_{50}). (A) Measurement of caspase 8 activation. (*) $p < 0.05$ vs negative control. (B) Measurement of caspase 3 activation. (*) $p < 0.05$ vs negative control. (C) Cell cycle analysis. panel 1, negative control (DMSO-treated cells); panel 2, complex **1a**; panel 3, complex **2a**. Percentages of cells on each phase are included.

drug that triggers extrinsic apoptosis on a colorectal cancer model.

Lastly, cell cycle distribution upon 48 h of incubation with both complexes **1a** and **2a** was studied. Cell cycle arrest might be indicative of DNA damage and is usually considered as an apoptotic biomarker as well.[69,70] Treatment with both complexes induced cell cycle arrest on the G_1 phase (Figure 5C); gold(I) derivative **1a** triggered a more pronounced arrest than its silver(I) counterpart, which is in accordance with the data previously obtained which suggest that **1a** might be faster than **2a** with regard to its cell death induction capacity.

https://dx.doi.org/10.1021/acs.inorgchem.0c02922
Inorg. Chem. XXXX, XXX, XXX−XXX

*2.3.3. Gold(I) Complex **1a** and Silver(I) Complex **2a** Disruption of Mitochondrial Function.* In order to determine the effect of both **1a** and **2a** complexes on mitochondrial function, we analyzed mitochondrial integrity in terms of changes in the mitochondrial membrane potential. After 48 h incubation with the IC_{50} value of gold(I) and silver(I) derivatives, respectively, we noticed a significant loss on $\Delta\psi$ (Figure 6A). Given that loss of mitochondrial membrane potential might be related to mitochondrial dysfunction and aberrant ROS production, we then measured ROS levels after 24 h incubation with both metallodrugs. A significant ($p < 0.05$) increase in this parameter was found only upon treatment with the gold complex **1a** (Figure 6B).

Cancer cells have a quite delicate redox balance, and redox homeostasis disruption has been proposed as a promising anticancer approach.[71] In light of results shown on Figure 6B, we evaluated the role of ROS on cell death triggered by complexes **1a** and **2a** using the ROS scavenger N-acetylcysteine (NAC). Pretreatment of Caco-2 cells with NAC resulted in a partial recovery of cell viability decrease induced by complex **1a**, but no modification of cell viability was detected in the cell culture treated with the silver derivative **2a** (Figure 6C). Given that we have previously observed that our silver-containing drug did not disturb redox homeostasis (Figure 6B), this result was not unexpected. Therefore, our results suggest that the silver(I) complex **2a** might trigger ROS-independent apoptosis on Caco-2 cells. Given that pro-oxidant chemotherapeutic agents might damage noncancer tissues as well, novel drugs able to induce ROS-independent cell death are currently of great interest;[72] thus, $[Ag(TfO)(L1)(PPh_3)]$ (**2a**) might be strongly considered as a future anticancer drug.

It is also noticeable that treatment with complex **2a** resulted in a greater loss of $\Delta\psi$ than its gold(I) counterpart and might be related to its mechanism of action. According to data from Eloy et al., silver(I) complexes might accumulate on mitochondria and induce mitochondrial dysfunction as a consequence, leading to the release of AIF (apoptosis-inducing factor) and cell death via apoptosis. Moreover, authors reported that mitochondrial dysfunction was not accompanied by redox balance disruption,[73] which is in accordance with our current findings.

On the other hand, pretreatment with NAC did not fully recover Caco-2 cells incubated with the gold(I) complex **1a**, which suggests that ROS generation might be a part of its mechanism of action, and a ROS-independent cell death mechanism is also involved.

2.3.4. Gold(I) Complex Inhibition of TrxR and 20S Proteasome. Redox enzyme thioredoxin reductase (TrxR) is one of the main targets of gold(I) derivatives, given the affinity between the gold atom and the selenocysteine residue located on the active site of the protein.[3] Therefore, we measured TrxR activity on Caco-2 cell lysates after 24 h incubation with complex **1a**. We also performed TrxR enzymatic activity assay upon 24 h incubation with silver-containing complex **2a**, since some authors have reported that silver(I) might be able to inhibit this redox enzyme.[74] As can be observed on Figure 7A, treatment with the gold derivative **1a** resulted in a significant ($p < 0.05$) decrease in TrxR activity, whereas no changes were observed upon treatment with the silver compound **2a**. Inhibition of TrxR might be related to the increase in ROS levels found upon treatment with complex **1a** (Figure 7B). In line with this, the lack of TrxR inhibition after treatment with

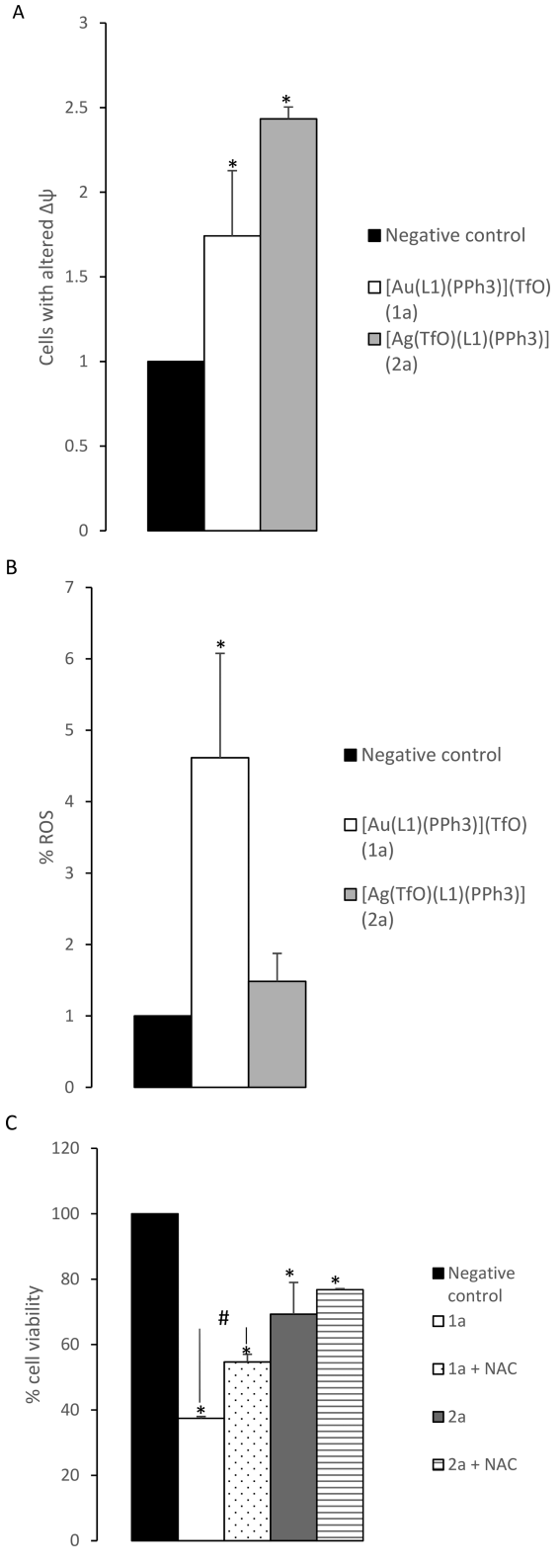

Figure 6. Effect of complexes **1a** and **2a** on mitochondrial integrity and ROS levels of Caco-2 cells. (A) Analysis of mitochondrial membrane potential after 48 h incubation with **1a** and **2a** (IC_{50}). (*) $p < 0.05$ vs negative control. (B) Measurement of ROS levels after 24 h incubation with **1a** and **2a** (IC_{50}). (*) $p < 0.05$ vs negative control. (C) Percentage of cell viability after 24 h with **1a** and **2a** (IC_{50}) in the presence or absence of NAC (1 h, 30 mM). (*) $p < 0.05$ vs negative control. (#) $p < 0.05$ vs lack of NAC.

https://dx.doi.org/10.1021/acs.inorgchem.0c02922
Inorg. Chem. XXXX, XXX, XXX−XXX

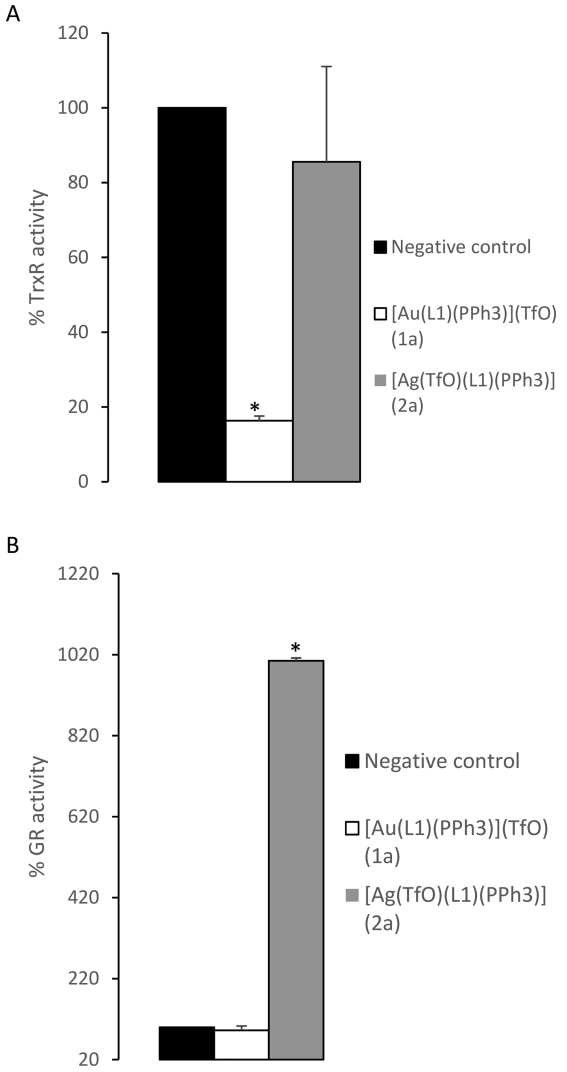

Figure 7. Effect of 24 h of treatment with complexes **1a** and **2a** (IC_{50}) on redox enzymes in Caco-2 cells. (A) Measurement of thioredoxin reductase activity (TrxR). (*) $p < 0.05$ vs negative control. (B) Measurement of glutathione reductase (GR). (*) $p < 0.05$ vs negative control.

2a might be in accordance with the absence of redox homeostasis disturbances and the consequent ROS-independent cell death triggered by the silver(I) complex.

In order to determine whether complex **1a** was able to selectively inhibit TrxR or might interact with further redox enzymes, we analyzed glutathione reductase (GR) activity on Caco-2 cell lysates upon 24 h incubation with **1a**. In addition, GR activity was measured on Caco-2 cells treated with complex **2a** to compare the effect of both metallodrugs, whereas incubation with gold derivative **1a** resulted in no modifications of GR activity, which suggests that this complex might act as a selective TrxR inhibitor; treatment with silver(I) complex **2a** led to a great increase in glutathione reductase activity (Figure 7B). Cancer cells might increase GR expression and/or activity as a chemoresistance mechanism in order to avoid cell death.[75] However, our results show how the strong increase in GR activity could break the redox equilibrium by modifying the mitochondrial potential and activating the caspases that lead to apoptosis.

Selective TrxR inhibition and the subsequent increase in ROS levels might not be the only mechanism of action of **1a** according to results shown in Figure 6C, since pretreatment with the ROS scavenger NAC did not fully recover cell viability. Therefore, we hypothesized a likely inhibition of proteasome as a further molecular target, which was feasible according to previous research.[76,77] We measured 20S proteasome activity on Caco-2 cells treated for 24 h with complexes **1a** and **2a**, respectively. Incubation with the gold(I) complex **1a** resulted in a significant ($p < 0.05$) decrease of chymotrypsin-like activity, thus suggesting that **1a** is able to inhibit 20S proteasome as well as TrxR (Figure 8). Taken together, our results suggest that [Au(L1)(PPh_3)](TfO) (**1a**) might act as a multitarget anticancer complex.

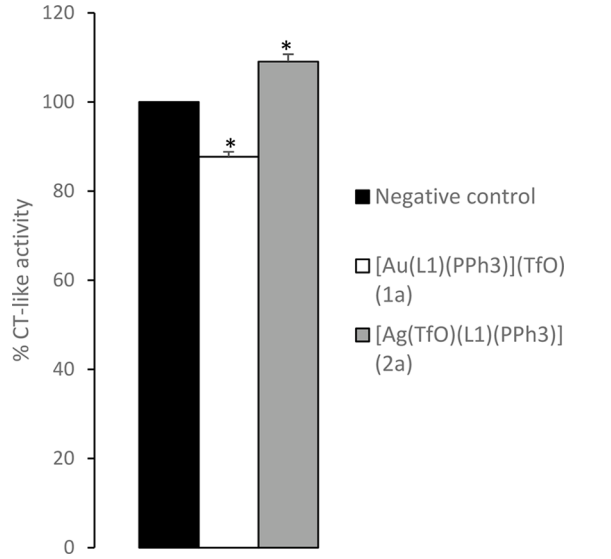

Figure 8. Determination of proteasomal chymotrypsin-like (CT-like) activity on Caco-2 cells upon 24 h treatment with complexes **1a** and **2a** (IC_{50}). (*) $p < 0.05$ vs negative control.

Contrarily, treatment with the silver(I) derivative **2a** triggered an increase in chymotrypsin-like activity, which discards a likely inhibition of proteasome protease capacity as mechanism of action. On the other hand, this unexpected finding might be related with the previously discussed increase in GR activity upon treatment with **2a**, since it has been reported that an increase in proteasomal activity might lead to an overexpression of glutathione reductase along with other antioxidant enzymes.[78]

3. CONCLUSION

Herein we have described and characterized two heterocyclic ligands derived 2-anilinopyridine, together with the two families of mononuclear gold(I) and mono- and dinuclear silver(I) derivatives. Both gold-containing complexes [Au(L1)(PPh_3)](TfO) (**1a**) and [Au(L2)(PPh_3)](TfO) (**1b**) displayed great antiproliferative activity toward a model of colorectal adenocarcinoma (Caco-2 cell line) and two breast adenocarcinoma cancer cell lines (MCF-7 and MDA-231). Furthermore, the complex [Au(L1)(PPh_3)](TfO) (**1a**) induced caspases 8 and 3 activation, loss of mitochondrial membrane potential, and ROS-dependent cell death on Caco-2 cells upon 24 h incubation. Regarding its mechanism of action, the complex exhibits a significant inhibition of redox enzyme

https://dx.doi.org/10.1021/acs.inorgchem.0c02922
Inorg. Chem. XXXX, XXX, XXX−XXX

thioredoxin reductase as well as 20S proteasome. On the other hand, silver complexes also showed good cytotoxic activity and the effect of the silver(I) analogue [Ag(TfO)(L1)(PPh_3)] (**2a**) on Caco-2 cells was evaluated. This derivative triggered ROS-independent apoptosis mediated by caspase 8 and 3 activation and loss of mitochondrial membrane potential. However, cell death is not mediated either by inhibition of the enzyme thioredoxin reductase or 20S proteasome; instead, the silver-containing drug might disrupt mitochondrial function and increase in the activity of the GR according to our current data. Further studies will be needed to validate this hypothesis. In conclusion, we have observed that these new gold(I) and silver(I) complexes might not be able to interact with the same molecular targets, thus triggering different modes of cell death.

Trying to evaluate the structure activity relationship in these compounds, we may conclude that although ligand L1 is less active than L2, their complexes are more active in general and within them those bearing gold and triphenylphosphine are the most active. The silver complexes do not show a clear tendency because of for L1 the dimeric species with tryphenylphosphine exhibit excellent activities in both cell lines; however, for L2 the complexes bearing two ligands coordinated to the metallic center are the most active.

4. EXPERIMENTAL SECTION

4.1. General Method. Solvents were used as received without purification or drying. The starting materials [Ag(TfO)(PPh_3)][79] and [Au(TfO)(PPh_3)] were obtained by reaction of [AuCl(PPh_3)] with Ag(TfO) in dichloromethane and used "in situ". All other reagents were commercially available and used without further purification. ^{1}H, ^{13}C{^{1}H}, ^{19}F{^{1}H}, and ^{31}P{^{1}H} NMR spectra, including 2D experiments, were recorded on a Bruker Avance 400 or a Bruker ARX 300 spectrometers. Chemical shifts (δ, ppm) were reported relative to the solvent peaks in the ^{1}H, ^{13}C spectra or external 85% H_3PO_4 or $CFCl_3$ in ^{31}P or ^{19}F spectra. IR spectra were recorded in the range 4000−200 cm^{-1} on a PerkinElmer Spectrum 100 spectrophotometer on solid samples using an ATR accessory. C, H, and N analyses were carried out with a PerkinElmer 2400 Series 2 microanalyzer. Mass spectra were recorded on a VG Austopec, with the ESI technique.

4.2. Synthesis of the Ligands {(4-pyCO)N(Ph)(py)} (L1) and {(2-(C_4H_4S)CO)N(Ph)(py)} (L2). To a dichloromethane solution (10 mL) of 2-anilinopyridine (0.3404 g, 2 mmol) under argon atmosphere was added NEt_3 (0.2626 g, 2.6 mmol) and 4-chlorocarbonylpyridine (0.3560 g, 2 mmol) or 2-chlorocarbonylthiophene (0.2932 g, 2 mmol). The reaction was stirred for 24 h at room temperature. The solution was washed with a saturated solution of $NaHCO_3$ and then washed with dichloromethane (3 × 20 mL) and dried with anhydrous $MgSO_4$. Then the solution was filtered through Celite, and the solution was reduced to minimum volume under vacuum. The addition of *n*-hexane afforded a white solid which was filtered off and washed with *n*-hexane.

*4.2.1. {(4-pyCO)N(Ph)(py)} (**L1**).* White solid in 56% yield. ^{1}H NMR (400 MHz, $(CD_3)_2CO$, 25 °C; ppm): δ 8.50 (m, 2H, H$^{2'',6''}$); 8.27 (m, 1H, H$^{6'}$); 7.82 (m, 1H, H$^{4'}$); 7.42 (m, 1H, H$^{3'}$); 7.36 (m, 4H, H$^{3'',5''}$, Ph); 7.29 (m, 3H, Ph); 7.22 (m, 1H, H$^{5'}$). ^{13}C{^{1}H} NMR (100 MHz, $(CD_3)_2CO$; ppm): δ 156.6 (C$^{2'}$); 150.6 (C$^{2'',6''}$); 149.5 (C$^{6'}$); 145.3 (C^1); 143.1 (C$^{4''}$); 139.1 (C$^{4'}$); 130.0 (C^{2,6}); 128.9 (C^4); 127.9 (C^{3,5}); 123.1 (C$^{3'}$); 122.8 (C$^{3'',5''}$); 122.4 (C$^{5'}$). IR: ν(C═O) 1652 cm^{-1}. Elem. Anal. Calcd (%) for $C_{17}H_{13}N_3O$ (275.30): C, 74.17; H, 4.76; N, 15.26. Found: C, 74.04; H, 4.26; N, 15.41. MS (ESI$^+$): [L1 + H]$^+$ *m*/*z* 276 (100%); [2L1 + Na]$^+$ *m*/*z* 573 (45%).

*4.2.2. {(2-(C_4H_4S)CO)N(Ph)(py)} (**L2**).* White solid in 52% yield. ^{1}H NMR (400 MHz, $(CD_3)_2CO$, 25 °C; ppm): δ 8.38 (m, 1H, H$^{6'}$); 7.85 (m, 1H, H$^{4'}$); 7.62 (dd, 1H, J_{H-H} = 5.0; 1.2 Hz, H$^{5''}$); 7.51 (m, 1H, H$^{3'}$); 7.42 (m, 2H, H^{2,6}); 7.33 (m, 3H, H^{3,4,5}); 7.27 (m, 1H, H$^{5'}$); 6.91 (m, 1H, H$^{4''}$); 6.82 (dd, 1H, J_{H-H} = 3.8;1.2 Hz, H$^{3''}$). ^{13}C{^{1}H} NMR (100 MHz, $(CD_3)_2CO$; ppm): δ 150.1 (C$^{6'}$); 139.3 (C$^{4'}$); 133.4 (C$^{3''}$); 132.6 (C$^{5''}$); 130.4 (C^{2,6}); 129.8 (C^4); 128.5 (C^{3,5}); 128.2 (C$^{4''}$); 123.4 (C$^{3'}$); 123.2 (C$^{5'}$). IR: ν(C═O) 1655 cm^{-1}. Elem. Anal. Calcd (%) for $C_{16}H_{12}N_2OS$ (280.34): C, 68.55; H, 4.31; N, 9.99; S, 11.44. Found: C, 67.84; H, 4.21; N, 9.92; S, 10.87. MS (ESI$^+$): [L1 + H]$^+$ *m*/*z* 276 (100%); [2L1 + Na]$^+$ *m*/*z* 573 (45%). MS(ESI+): [L2 + H]$^+$ *m*/*z* = 281 (100%).

4.3. Synthesis of Complexes [Au(L)(PPh_3)](TfO) (L1, 1a; L2, 1b). To a dichloromethane solution (10 mL) of [AuCl(PPh_3)] (0.1484 g, 0.3 mmol) was added [Ag(TfO)] (0.0848 g, 0.33 mmol). After 45 min of stirring protected from light, the white solid (AgCl) was filtered through Celite and the solution was added to dichloromethane solution (10 mL) of L1 (0.0743 g, 0.27 mmol) or L2 (0.0757 g, 0.27 mmol). The reaction was stirred for 2 h at room temperature. Then the solution was reduced to minimum volume under vacuum. A white solid was obtained and washed with *n*-hexane.

*4.3.1. [Au(L1)(PPh_3)](TfO) (**1a**).* White solid in 91% yield. ^{1}H NMR (400 MHz, $(CD_3)_2CO$, 25 °C; ppm) δ 8.86 (d, 2H, J_{H-H} = 5.8 Hz, H$^{2'',6''}$); 8.32 (m, 1H, H$^{6'}$); 7.90 (m, 1H, H$^{4'}$); 7.82 (d, 2H, J_{H-H} = 6.0 Hz, H$^{3'',5''}$); 7.65 (m, 15H, PPh_3); 7.49 (d, 1H, J_{H-H} = 8.1 Hz, H$^{3'}$); 7.43 (m, 2H, Ph); 7.35 (m, 3H, Ph); 7.31 (m, 1H, H$^{5'}$). ^{19}F{^{1}H} NMR (100 MHz, $(CD_3)_2CO$; ppm): δ −80.1 (s). ^{31}P{^{1}H} NMR (100 MHz, $(CD_3)_2CO$; ppm): δ 29.9 (s). ^{13}C{^{1}H} NMR (100 MHz, $(CD_3)_2CO$; ppm): δ δ: 152.5 (C$^{2'',6''}$); 149.9 (C$^{6'}$); 142.2 (s); 135.2 (d, 6C, J_{C-C} = 13.7 Hz, PPh_3); 133.6 (m, 3C, PPh_3); 130.6 (d, 6C, J_{C-C} = 12.1 Hz, PPh_3); 130.3 (C^{2,6}); 129.0 (C^4); 128.7 (C^{3,5}); 128.1 (s); 125.8 (C$^{3'',5''}$); 123.6 (s, C$^{3'}$ or C$^{5'}$). IR (cm^{-1}): ν(C═O) 1653; ν_{as}(SO_3) 1261; ν_s(CF_3) 1220; ν_{as}(CF_3) 1143; ν_s(SO_3) 1030. Elem. Anal. Calcd (%) for $C_{36}H_{28}AuF_3N_3O_4PS$ (883.63): C, 48.93; H, 3.19; N, 4.76; S, 3.63. Found: C, 48.33; H, 2.96; N, 4.38; S, 3.24. MS (ESI+): [L1 + H]$^+$ *m*/*z* 276 (100%); [M − TfO]$^+$ *m*/*z* 734 (17%); [Au(PPh_3)$_2$]$^+$ *m*/*z* 721 (65%).

*4.3.2. [Au(L2)(PPh_3)](TfO) (**1b**).* White solid in 60% yield. ^{1}H NMR (400 MHz, $(CD_3)_2CO$, 25 °C; ppm): δ 9.09 (m, 1H, H$^{6'}$); 8.48 (td, 1H, J_{H-H} = 7.9; 1.7 Hz, H$^{4'}$); 7.94 (m, 2H, H$^{3',5'}$); 7.66−7.44 (m, 21H, H$^{5''}$+PPh_3); 6.81 (dd, 1H, J_{H-H} = 3.9; 1.2 Hz, H$^{3''}$); 6.76 (m, 1H, H$^{4''}$). ^{19}F{^{1}H} NMR (100 MHz, $(CD_3)_2CO$; ppm): δ −80.1 (s). ^{31}P{^{1}H} NMR (100 MHz, $(CD_3)_2CO$; ppm): δ 30.1 (s). ^{13}C{^{1}H} NMR (100 MHz, $(CD_3)_2CO$; ppm): δ δ: 164.51 (s, 1C, C═O); 156.9 (s); 152.6 (C$^{6'}$); 145.3 (C$^{4'}$); 142.3 (s); 137.5 (s); 135.0 (d, 6C, J_{C-C} = 13.6 Hz, PPh_3); 134.7 (C$^{3''}$); 134.3 (C$^{5'}$); 133.5 (m, 2C, PPh_3); 131.0 (C^{2,6}); 130.5 (d, 6C, J_{C-C} = 12.1 Hz, PPh_3); 129.7 (C^4); 129.1 (C^{3,5}); 128.5 (C$^{4''}$); 127.6 (C$^{3'}$); 126.0 (C$^{5'}$). IR (cm^{-1}): ν(C═O) 1631, ν_{as}(SO_3) 1257; ν_s(CF_3) 1225; ν_{as}(CF_3) 1150; ν_s(SO_3) 1029. Elem. Anal. Calcd (%) for $C_{35}H_{27}AuF_3N_2O_4PS_2$ (888.67): C, 47.30; H, 3.06; N, 3.15; S, 7.22. Found: C, 47.8; H, 2.93; N, 3.62; S, 6.94. MS (ESI+): [L2 + H]$^+$ *m*/*z* 281 (8%); [Au(PPh_3)$_2$]$^+$ *m*/*z* 721 (100%).

4.4. Synthesis of Complexes [Ag(TfO)(L)(PPh_3)] (L1, 2a; L2, 2b). To a dichloromethane solution (10 mL) of [Ag(TfO)(PPh_3)] (0.1557 g, 0.3 mmol) was added L1 or L2 (0.3 mmol). After 45 min of stirring protected from light at room temperature, the solution was reduced to minimum volume under vacuum. A white solid was obtained and washed with *n*-hexane.

*4.4.1. [Ag(TfO)(L1)(PPh_3)] (**2a**).* White solid in 52% yield. ^{1}H NMR (400 MHz, $(CD_3)_2CO$, 25 °C; ppm): δ 8.66 (m, 2H, H$^{2'',6''}$); 8.34 (m, 1H, H$^{6'}$); 7.89 (m, 1H, H$^{4'}$); 7.55 (m, 17H, H$^{3'',5''}$+PPh_3); 7.48 (d, 1H, J_{H-H} = 8.1 Hz, H$^{3'}$); 7.39 (m, 2H, Ph); 7.33 (m, 4H, H^5+Ph). ^{19}F{^{1}H} NMR (100 MHz, $(CD_3)_2CO$; ppm): δ −77.9 (s). ^{31}P{^{1}H} NMR (100 MHz, $(CD_3)_2CO$, 203 K; ppm): δ 13.7 (2d, $J_{109Ag-P}$ = 762.8 Hz, $J_{107Ag-P}$ = 661.0 Hz, $AgPPh_3$). ^{13}C{^{1}H} NMR (100 MHz, $(CD_3)_2CO$; ppm): δ δ: 156.3 (s); 151.8 (C$^{2'',6''}$); 149.9 (C$^{6'}$); 142.6 (m); 139.7 (C$^{4'}$); 134.8 (d, 6C, J_{C-C} = 15.8 Hz, PPh_3); 132.1 (3C, PPh_3); 131.4 (d, 3C, J_{C-C} = 41.4 Hz, PPh_3); 130.2 (m, 6C, PPh_3); 130.2 (C^{2,6}); 128.9 (C^4); 128.3 (C^{3,5}); 123.2 (C$^{3'',5''}$); 122.7 (C$^{3',5'}$). IR (cm^{-1}): ν(C═O) 1635; ν_{as}(SO_3) 1246; ν_s(CF_3) 1224; ν_{as}(CF_3) 1145; ν_s(SO_3) 1026. Elem. Anal. Calcd (%) for $C_{36}H_{28}AgF_3N_3O_4PS$ (794.53): C, 54.42; H, 3.55; N, 5.29, S, 4.04. Found: C, 54.47; H,

https://dx.doi.org/10.1021/acs.inorgchem.0c02922
Inorg. Chem. XXXX, XXX, XXX−XXX

3.71; N, 5.18; S, 4.44. MS (ESI+): $[Ag(PPh_3)_2]^+$ m/z 633 (100%); $[M - TfO]^+$ m/z 646 (25%).

*4.4.2. [Ag(TfO)(L2)(PPh$_3$)] (**2b**).* White solid in 68% yield. ^{1}H NMR (400 MHz, $(CD_3)_2CO$, 25 °C; ppm): δ 8.39 (m, 1H, H$^{6'}$); 7.87 (m, 1H, H$^{4'}$); 7.63 (dd, 1H, J_{H-H} = 5.0; 1.2 Hz, H$^{5''}$); 7.57 (m, 3H, H$^{2,6,3'}$); 7.47 (m, 15H, PPh_3); 7.34 (m, 3H, H^{3,4,5}); 7.28 (m, 1H, H$^{5'}$); 6.91 (m, 1H, H$^{4''}$); 6.82 (dd, 1H, J_{H-H} = 3.8; 1.2 Hz, H$^{3''}$). ^{19}F{^{1}H} NMR (100 MHz, $(CD_3)_2CO$; ppm): δ −78.7 (s). ^{31}P{^{1}H} NMR (100 MHz, $(CD_3)_2CO$, 203 K; ppm): δ 10.1 (2m, 1P, $J_{109Ag-P}$ = 533.3 Hz, $J_{107Ag-P}$ = 463.1 Hz). ^{13}C{^{1}H} NMR (100 MHz, $(CD_3)_2CO$; ppm): δ 149.9 (s); 139.2 (s); 134.7 (d, 6C, J_{C-C} = 15.5 Hz, PPh_3); 133.2 (s); 132.3 (s); 132.0 (s, 3C, PPh_3); 131.5 (s); 130.2 (s, 6C, PPh_3); 129.4 (s); 128.2 (s); 127.8 (s); 123.2. IR (cm^{-1}): ν(C═O) 1625; $\nu_{as}(SO_3)$ 1265; $\nu_s(CF_3)$ 1221; $\nu_{as}(CF_3)$ 1141; $\nu_s(SO_3)$ 1026. Elem. Anal. Calcd (%) for $C_{35}H_{27}AgF_3N_2O_4PS_2$ (799.57): C, 52.58; H, 3.40; N, 3.50; S, 8.02. Found: C, 52.30; H, 3.41; N, 3.23; S, 8.34. MS (ESI+): $[Ag(PPh_3)_2]^+$ m/z 633 (100%); $[M - TfO]^+$ m/z 651 (13%).

4.5. Synthesis of Complexes [Ag$_2$(TfO)$_2$(L)(PPh$_3$)$_2$] (L1, 3a; L2, 3b). To a dichloromethane solution (10 mL) of [Ag(TfO)-(PPh_3)] (0.1557 g, 0.6 mmol) was added L1 or L2 (0.3 mmol). After 45 min of stirring protected from light at room temperature, the solution was reduced to minimum volume under vacuum. A white solid was obtained and washed with *n*-hexane.

*4.5.1. [Ag$_2$(TfO)$_2$(L1)(PPh$_3$)$_2$] (**3a**).* White solid in 78% yield. ^{1}H NMR (400 MHz, $(CD_3)_2CO$, 25 °C; ppm) δ 8.71 (m, 2H, H$^{2'',6''}$); 8.47 (m, 1H, H$^{6'}$); 7.96 (m, 1H, H$^{4'}$); 7.54 (m, 33H, H$^{3',3'',5''}$+PPh_3); 7.35 (m, 5H, Ph); 7.27 (m, 1H, H$^{5'}$). ^{19}F{^{1}H} NMR (100 MHz, $(CD_3)_2CO$; ppm): δ −79.9 (s). ^{31}P{^{1}H} NMR (100 MHz, $(CD_3)_2CO$, 203 K; ppm): δ 13.1 (2d, $J_{109Ag-P}$ = 927.9 Hz, $J_{107Ag-P}$ = 838.8 Hz, $AgPPh_3$). ^{13}C{^{1}H} NMR (100 MHz, $(CD_3)_2CO$; ppm): δ 152.1 (C$^{2'',6''}$); 150.4 (C$^{6'}$); 142.6 (m); 140.3 (C$^{4'}$); 134.8 (m, 12C, PPh_3); 132.1 (6C, PPh_3); 130.4 (C^{2,6}); 130.2(m, 12C, PPh_3); 128.8 (C^4); 128.5 (C^{3,5}); 124.5 (py); 123.5 (py); 123.4 (py). IR (cm^{-1}): ν(C═O) 1667; $\nu_{as}(SO_3)$ 1239; $\nu_s(CF_3)$ 1220; $\nu_{as}(CF_3)$ 1149; $\nu_s(SO_3)$ 1023. Elem. Anal. Calcd (%) for $C_{55}H_{43}Ag_2F_6N_3O_7P_2S_2$ (1313.75): C, 50.28; H, 3.30; N, 3.20; S, 4.88. Found: C, C, 50.68; H, 3.62; N, 3.43; S, 4.35. MS (ESI+): $[Ag(PPh_3)_2]^+$ m/z 633 (100%); $[M - Ag - 2TfO]^+$ m/z 646 (50%).

*4.5.2. [Ag$_2$(TfO)$_2$(L2)(PPh$_3$)$_2$] (**3b**).* White solid in 44% yield. ^{1}H NMR (400 MHz, $(CD_3)_2CO$, 25 °C; ppm): δ 8.62 (m, 1H, H$^{6'}$); 8.04 (m, 1H, H$^{4'}$); 7.58 (m, 32H, H$^{3',5''}$+PPh_3); 7.47 (m, 1H, H$^{5'}$); 7.39 (m, 4H, Ph); 7.36 (m, 1H, Ph); 6.85 (m, 1H, H$^{4''}$); 6.78 (dd, 1H, J_{H-H} = 3.8 1.2 Hz, H$^{3''}$). ^{19}F{^{1}H} NMR (100 MHz, $(CD_3)_2CO$; ppm): δ −80 (s). ^{31}P{^{1}H} NMR (100 MHz, $(CD_3)_2CO$, 203 K; ppm): δ 13.0 (2m, 1P, $J_{Ag-P\ (av)}$ = 725.5 Hz, $SAgPPh_3$); 10.6 (2m, $J_{Ag-P\ (av)}$ = 520.9 Hz, $NAgPPh_3$). ^{13}C{^{1}H} NMR (100 MHz, $(CD_3)_2CO$; ppm): δ 151.4 (C$^{6'}$); 141.7 (C$^{4'}$); 134.8 (m, 6C, PPh_3); 134.0 (C$^{3''}$); 133.3 (C$^{5''}$); 132.1 (s, 3C, PPh_3); 130.7 (s, 2C, C^{2,6}); 130.2 (s, 6C, PPh_3); 129.1 (C^4); 129.0 (s, 2C, C^{3,5}); 128.1 (C$^{4''}$); 125.0 (C$^{3'}$); 124.0 (C$^{5'}$). IR (cm^{-1}): ν(C═O) 1638; $\nu_{as}(SO_3)$ 1239; $\nu_s(CF_3)$ 1220; $\nu_{as}(CF_3)$ 1148; $\nu_s(SO_3)$ 1023. Elem. Anal. Calcd (%) for $C_{54}H_{42}Ag_2F_6N_3O_7P_2S$ (1318.79): C, 49.18; H, 3.21; N, 2.12; S, 7.29. Found: C, 49.01; H, 3.25; N, 1.99; S, 6.98. MS (ESI+): $[Ag(PPh_3)_2]^+$ m/z 633 (100%); $[L2 + Ag(PPh_3)]^+$ m/z 651 (61%).

4.6. Synthesis of Complexes [Ag(TfO)(L)]$_2$ (L1, 4a; L2, 4b). To a dichloromethane solution (10 mL) of [Ag(TfO)] (0.051 g, 0.2 mmol) was added L1 or L2 (0.2 mmol). After 45 min of stirring protected from light at room temperature, the solution was reduced to minimum volume under vacuum. A white solid was obtained and washed with *n*-hexane.

*4.6.1. [Ag(TfO)(L1)]$_2$ (**4a**).* White solid in 72% yield. ^{1}H NMR (400 MHz, $(CD_3)_2CO$, 25 °C; ppm): δ 8.56 (m, 4H, H$^{2'',6''}$); 8.30 (m, 2H, H$^{6'}$); 7.86 (td, 2H, J_{H-H} = 7.9; 2.0 Hz, H$^{4'}$); 7.45 (m, 6 H, H$^{3',3'',5''}$); 7.39 (m, 4H, *Ph*); 7.29 (m, 8H, H$^{5'}$+Ph). ^{19}F{^{1}H} NMR (100 MHz, $(CD_3)_2CO$; ppm): δ −77.8 (s). ^{13}C{^{1}H} NMR (100 MHz, $(CD_3)_2CO$; ppm): δ 168.0 (s, 2C, C═O); 154.8 (s, 2C); 149.9 (4C, C$^{2'',6''}$); 148.8 (C$^{6'}$); 144.6 (s, 2C); 141.1 (s, 2C); 138.8 (s, 2C, C$^{4'}$); 129.3 (s, 4C, C^{2,6}); 128.0 (C^4); 122.7 (C$^{3',5'}$); 122.6 (s, 2C); 122.4 (s, 2C); 121.9 (s,2C). IR (cm^{-1}): ν(C═O) 1659; $\nu_{as}(SO_3)$ 1248; $\nu_s(CF_3)$ 1221; $\nu_{as}(CF_3)$ 1141; $\nu_s(SO_3)$ 1026. Elem. Anal. Calcd (%) for $C_{36}H_{26}Ag_2F_6N_6O_8S_2$ (1064.48): C, 40.62; H, 2.46; N, 7.89; S, 6.02. Found: C, 39.98; H, 2.40; N, 7.81; S, 5.98. MS (ESI+): $[L1 + H]^+$ m/z 276 (100%); $[M - 2TfO - Ag]^+$ m/z 657 (99%); $[M - TfO + Na]^{2+}$ m/z 938 (8%).

*4.6.2. [Ag(TfO)(L2)]$_2$ (**4b**).* White solid in 16% yield. ^{1}H NMR (400 MHz, $(CD_3)_2CO$, 25 °C; ppm) δ 8.88 (m, 2H, H$^{6'}$); 8.52 (M, 2H, H$^{4'}$); 7.86 (m, 4 H, H$^{5',5''}$); 7.71 (m, 10H, *Ph*); 7.38 (d, 2H, J_{H-H} = 8.4 Hz, H$^{3'}$); 7.01 (m, 4H, H$^{3'',4''}$). ^{19}F{^{1}H} NMR (100 MHz, $(CD_3)_2CO$;): δ −80.0 (s). ^{13}C{^{1}H} NMR (100 MHz, $(CD_3)_2CO$; ppm): δ 165.3 (s, 2C); 153.1 (s, 2C); 147.0 (s, 2C, C$^{4'}$); 136.4 and 128.6 (m, 4C, C$^{3'',4''}$); 136.0 (s, 2C, C$^{5'}$ or C$^{5''}$), 131.9 (s, 4C, C^{2,6}); 131.6 (C^4); 130.7 (s, 4C, C^{3,5}). IR (cm^{-1}): ν(C═O) 1644; $\nu_{as}(SO_3)$ 1256; $\nu_s(CF_3)$ 1221; $\nu_{as}(CF_3)$ 1146; $\nu_s(SO_3)$ 1023. Elem. Anal. Calcd (%) for $C_{34}H_{24}Ag_2F_6N_4O_8S_4$ (1074.56): C, 38.00; H, 2.25; N, 5.21; S, 11.94. Found: C, 38.28; H, 2.20; N, 4.88; S, 11.99. MS (ESI+): $[L2 + H]^+$ m/z 281 (100%).

4.7. Synthesis of Complexes [Ag(TfO)(L)$_2$] (L1, 5a; L2, 5b). To a dichloromethane solution (10 mL) of [Ag(TfO)] (0.051 g, 0.2 mmol) was added L1 or L2 (0.4 mmol). After 45 min of stirring protected from light at room temperature, the solution was reduced to minimum volume under vacuum. A white solid was obtained and washed with *n*-hexane.

*4.7.1. [Ag(TfO)(L1)$_2$] (**5a**).* White solid in 54% yield. ^{1}H NMR (400 MHz, $(CD_3)_2CO$, 25 °C; ppm): δ 8.54 (m, 4H, H$^{2'',6''}$); 8.28 (m, 2H, H$^{6'}$); 7.83 (m, 2H, H$^{4'}$); 7.39 (m, 10 H, H$^{3',3'',5''}$ + *Ph*); 7.28 (m, 6H, Ph); 7.23 (td, 2H, J_{H-H} = 4.9; 1.0 Hz, H$^{5'}$). ^{19}F{^{1}H} NMR (100 MHz, $(CD_3)_2CO$; ppm): δ −78.9 (s). ^{13}C{^{1}H} NMR (100 MHz, $(CD_3)_2CO$; ppm): δ δ: 150.5 (4C, C$^{2'',6''}$); 149.6 (C$^{6'}$); 139.3 (s, 2C, C$^{4'}$); 130.1 (s, 4C, C^{2,6}); 129.0 (C^4); 128.1 (s, 4C, C^{3,5}); 123.8 (s, 4C, C$^{3'',5''}$); 122.9 (s, 2C, C$^{3'}$); 122.4 (s, 2C, C$^{5'}$). IR (cm^{-1}): ν(C═O) 1654; $\nu_{as}(SO_3)$ 1251; $\nu_s(CF_3)$ 1222; $\nu_{as}(CF_3)$ 1154; $\nu_s(SO_3)$ 1027. Elem. Anal. Calcd (%) for $C_{35}H_{26}AgF_3N_6O_5S$ (807.55): C, 52.06; H, 3.25; N, 10.41; S, 3.97. Found: C, 52.55; H, 3.23; N, 10.39; S, 3.56. MS (ESI+): $[L1 + H]^+$ m/z 276 (45%); $[M - TfO]^+$ m/z 659 (100%).

*4.7.2. [Ag(TfO)(L2)$_2$] (**5b**).* White solid in 39% yield. ^{1}H NMR (400 MHz, $(CD_3)_2CO$, 25 °C) δ (ppm) = 8.51 (m, 2H, H$^{6'}$); 8.12 (m, 2H, H$^{4'}$); 7.56 (d, 2 H, J_{H-H} = 4.4 Hz, H$^{5''}$); 7.47 (m, 14H, H$^{3',5'}$ + *Ph*); 6.90 (m, 4H, H$^{3'',4''}$). ^{19}F{^{1}H} NMR (100 MHz, $(CD_3)_2CO$; ppm): δ −80.1 (s). ^{13}C{^{1}H} NMR (100 MHz, $(CD_3)_2CO$; ppm): δ 133.7 (s, 2C, C$^{5'}$), 130.9 (s, 4C, C^{2,6}); 129.5 (s, 2C, C^4); 129.4 (s, 4C, C^{3,5}); 128.2 (s, 2C, C$^{4'}$). IR (cm^{-1}): ν(C═O) 1646; $\nu_{as}(SO_3)$ 1258; $\nu_s(CF_3)$ 1222; $\nu_{as}(CF_3)$ 1150; $\nu_s(SO_3)$ 1027. Elem. Anal. Calcd (%) for $C_{33}H_{24}AgF_3N_4O_5S_3$ (817.63): C, 48.48; H, 2.96; N, 6.85; S, 11.77. Found: C, 48.52; H, 3.03; N, 6.92; S, 12.24. MS (ESI+): $[L2 + H]^+$ m/z 281 (100%); $[M - TfO]^+$ m/z 669 (1%); $[M + H]^+$ m/z 819 (1%);

4.8. Cell Culture. Human colorectal adenocarcinoma Caco-2 cells were kindly provided by Dr. Edith Brot-Laroche (Université Pierre et Marie Curie-Paris 6 UMR S872, Les Cordeliers, France). Human breast adenocarcinoma MCF-7 and MDA-231 cells were kindly provided by Carlos J. Ciudad and Dr. Verònica Noé (Departamento de Bioquímica y Fisiología, Facultad de Farmacia, Universidad de Barcelona, Spain). All cell lines were maintained in a humidified atmosphere of 5% CO_2 at 37 °C. Cells (passages 20−40) were grown in Dulbecco's modified Eagle's medium (DMEM; Gibco Invitrogen, Paisley, U.K.) supplemented with 20% fetal bovine serum, 1% non-essential amino acids, 1% penicillin (1000 U/mL), 1% streptomycin (1000 μg/mL), and 1% amphotericin (250 U/mL). Culture medium was replaced every 2 days, and cells were passaged enzymatically with 0.25% trypsin-1 mM EDTA and subcultured on 25 cm^2 flasks at a density of 2 × 10^4 cells/cm^2.

Experiments in undifferentiated Caco-2 cells as well as on MCF-7 and MDA-231 cells were performed 24 h postseeding. For assays on differentiated Caco-2 cells, cells were cultured on 96-well plates under standard culture conditions for 7−9 days, until reaching 80% confluence as confirmed by optic microscopy observance.

4.9. Cell Treatment. Complexes were initially solved on DMSO to a concentration of 20 mM and then diluted on cell culture without

https://dx.doi.org/10.1021/acs.inorgchem.0c02922
Inorg. Chem. XXXX, XXX, XXX−XXX

fetal bovine serum to the required work concentrations. For treatment, cell culture medium was replaced with medium containing complexes and cells were incubated at 37 °C for a variable time depending on the assay.

4.10. Cell Proliferation Assay and IC_{50} Calculation. MTT assay was performed as previously described by Mármol et al.[59]

For IC_{50} calculation, cells were grown in 96-well plates at a density of 4000 cells per well and incubated overnight at standard culture conditions. Then, cells were exposed to a range of concentrations of complexes (0−20 μM for complexes **1**−**5a** and **1**−**5b**; 10−100 μM for coordination ligands L1 and L2) for 72 h. Changes in cell proliferation were analyzed by MTT, and the obtained absorbance values were converted into percentage of growth inhibition. Absorbance was measured with SPECTROstar Nano (BMG Labtech).

4.11. Cell Death Studies. Caco-2 cells were grown at 25 cm^2 flasks at a density of 300.000 cells per flask and incubated overnight under standard culture conditions. Cells were then exposed to gold and silver complexes for 48 h, then collected, and stained with Annexin V-FITC by flow cytometry as previously described by Sánchez-de-Diego et al.[80]

4.12. Measurement of Caspase 8 and Caspase 3 Activation. Caco-2 cells were grown at 25 cm^2 flasks at a density of 300.000 cells per flask and incubated overnight under standard culture conditions. Cells were then exposed to gold and silver complexes for 24 h and collected for caspase 8 and 3 activity measurement.

Caspase 8 Assay Kit (Abcam; ab39700) was used for colorimetric determination of caspase 8 activation. Treated Caco-2 cells were manipulated according to manufacturer's instructions, and absorbance was measured at 400 nm with SPECTROstar Nano (BMG Labtech). Protein concentration was determined by Bradford method.

For caspase 3 activation measurement, Caspase 3Assay Kit, Colorimetric (Sigma-Aldrich; CASP-3-C) was used. Treated Caco-2 cells were manipulated according to the manufacturer's instructions, and absorbance was measured at 405 nm with SPECTROstar Nano (BMG Labtech). Protein concentration was determined by Bradford method.

4.13. Propidium Iodide Staining of DNA Content and Cell Cycle Analysis. Caco-2 cells were grown at 25 cm^2 flasks at a density of 300.000 cells per flask and incubated overnight under standard culture conditions. Cells were exposed to gold and silver complexes for 48 h and then collected, and changes in cell cycle were analyzed as previously described by Sánchez-de-Diego et al.[80]

4.14. Flow Cytometry Mitochondrial Membrane Potential Assay. Caco-2 cells were grown at 25 cm^2 flasks at a density of 300.000 cells per flask and incubated overnight under standard culture conditions. Cells were then exposed to gold and silver complexes for 48 h, and changes in $\Delta\psi$ were performed as previously described by Sánchez-de-Diego et al.[80]

4.15. Analysis of Total Cellular Oxidative Stress. Caco-2 cells cells were grown in 96-well plates at a density of 4000 cells per well, and after overnight incubation under standard culture conditions, were exposed to gold and silver complexes 24 h. Thereafter, measurement of total intracellular ROS levels was performed as previously described by Sánchez-de-Diego et al.[80] Fluorescence data were normalized with the percentage of cell viability determined by MTT.

4.16. Analysis of Thioredoxin Reductase Activity. Caco-2 cells cells were grown in 96-well plates at a density of 4000 cells per well, and after overnight incubation under standard culture conditions, were exposed to gold and silver complexes 24 h. Then, TrxR activity was determined as previously described by Mármol et al.[59] Absorbance was measured with SPECTROstar Nano (BMG Labtech).

4.17. Measurement of Glutathione Reductase Activity. Caco-2 cells were grown in 96-well plates at a density of 4000 cells per well and, after overnight incubation under standard culture conditions, were exposed to gold and silver complexes for 24 h. Analysis of GR activity was performed as previously described by Sánchez-de-Diego et al.[80] Absorbance was measured with SPECTROstar Nano (BMG Labtech).

4.18. Analysis of 20S proteasome activity. Caco-2 cells were grown at 25 cm^2 flasks at a density of 300.000 cells per flask and incubated overnight under standard culture conditions. Cells were exposed to gold and silver complexes for 24 h, then collected, and lysed with saponine and centrifuged at 13.000 rpm for 15 min at 4 °C. Supernatant was further analyzed with Proteasome 20S Activity Assay Kit (Sigma-Aldrich; MAK172) according the manufacturer's instructions. Fluorescence was measured with FLUOstar Omega (BMG Labtech).

4.19. Crystal Structure Determinations. Crystals were mounted in inert oil on glass fibers and transferred to the cold gas stream of a Smart APEX CCD diffractometer equipped with a low-temperature attachment. Data were collected using monochromated Mo Kα radiation (λ = 0.71073 Å), scan type ϖ. Absorption corrections based on multiple scans were applied using SADABS.[75] The structures were solved by direct methods and refined on F^2 using the program SHELXT-2016.[76] All non-hydrogen atoms were refined anisotropically. CCDC deposition numbers are 2020939 (L1), 2020940 (L2), 2020941 (**1a**), and 2020942 (**1b**).

■ ASSOCIATED CONTENT

Supporting Information

The Supporting Information is available free of charge at https://pubs.acs.org/doi/10.1021/acs.inorgchem.0c02922.

RMN spectra of all the complexes PDF)

Accession Codes

CCDC 2020939−2020942 contain the supplementary crystallographic data for this paper. These data can be obtained free of charge via www.ccdc.cam.ac.uk/data_request/cif, or by emailing data_request@ccdc.cam.ac.uk, or by contacting The Cambridge Crystallographic Data Centre, 12 Union Road, Cambridge CB2 1EZ, UK; fax: +44 1223 336033.

■ AUTHOR INFORMATION

Corresponding Authors

Elena Cerrada − *Departamento de Química Inorgánica, Instituto de Síntesis Química y Catálisis Homogénea-ISQCH, Universidad de Zaragoza-CSIC, 50009 Zaragoza, Spain;* orcid.org/0000-0003-2457-3674; Email: ecerrada@unizar.es

M. Concepción Gimeno − *Departamento de Química Inorgánica, Instituto de Síntesis Química y Catálisis Homogénea-ISQCH, Universidad de Zaragoza-CSIC, 50009 Zaragoza, Spain;* orcid.org/0000-0003-0553-0695; Email: gimeno@unizar.es

M. Jesús Rodríguez-Yoldi − *Departamento de Farmacología y Fisiología, Unidad de Fisiología. and CIBERobn, IIS Aragón, IA2, Universidad de Zaragoza, 50013 Zaragoza, Spain;* Email: mjrodyol@unizar.es

Authors

Inés Mármol − *Departamento de Química Inorgánica, Instituto de Síntesis Química y Catálisis Homogénea-ISQCH, Universidad de Zaragoza-CSIC, 50009 Zaragoza, Spain; Departamento de Farmacología y Fisiología, Unidad de Fisiología. and CIBERobn, IIS Aragón, IA2, Universidad de Zaragoza, 50013 Zaragoza, Spain*

Sara Montanel-Perez − *Departamento de Química Inorgánica, Instituto de Síntesis Química y Catálisis Homogénea-ISQCH, Universidad de Zaragoza-CSIC, 50009 Zaragoza, Spain*

https://dx.doi.org/10.1021/acs.inorgchem.0c02922
Inorg. Chem. XXXX, XXX, XXX−XXX

José Carlos Royo − *Departamento de Farmacología y Fisiología, Unidad de Fisiología. and CIBERobn, IIS Aragón, IA2, Universidad de Zaragoza, 50013 Zaragoza, Spain*

M. Dolores Villacampa − *Departamento de Química Inorgánica, Instituto de Síntesis Química y Catálisis Homogénea-ISQCH, Universidad de Zaragoza-CSIC, 50009 Zaragoza, Spain*

Complete contact information is available at: https://pubs.acs.org/10.1021/acs.inorgchem.0c02922

Notes

The authors declare no competing financial interest.

■ ACKNOWLEDGMENTS

We thank Centro de Investigación Biomédica de Aragón (CIBA), España for technical assistance: https://www.iacs.es/, use of Servicio General de Apoyo a la Investigación-SAI, Universidad de Zaragoza. We thank The Ministerio de Economía y Competitividad (Grants CTQ2016-75816-C2-1-P, PID2019-104379RB-C21, and SAF2016-75441-R), CIBER-OBN under Grant CB06/03/1012 of the Instituto Carlos III, European Grant Interreg/SUDOE (Redvalue, SOE1/PI/E0123), Red Multimetdrugs (Grant RED2018-102471-T), and Aragon Regional Government (Grants B16_R17 and E07_20R) for financial support.

■ REFERENCES

(1) Rabik, C. A.; Dolan, M. E. Molecular mechanisms of resistance and toxicity associated with platinating agents. *Cancer Treat. Rev.* **2007**, *33*, 9−23.

(2) Kelland, L. *Nat. Rev. Cancer* **2007**, *7*, 573−584.

(3) Bindoli, A.; Rigobello, M. P.; Scutari, G.; Gabbiani, C.; Casini, A.; Messori, L. Thioredoxin reductase: A target for gold compounds acting as potential anticancer drugs. *Coord. Chem. Rev.* **2009**, *253* (11−12), 1692−1707.

(4) McKeage, M. J.; Maharaj, L.; Berners-Price, S. J. Mechanisms of cytotoxicity and antitumor activity of gold(I) phosphine complexes: the possible role of mitochondria. *Coord. Chem. Rev.* **2002**, *232* (1−2), 127−135.

(5) de Almeida, A.; Oliveira, B. L.; Correia, J. D. G.; Soveral, G.; Casini, A. Emerging protein targets for metal-based pharmaceutical agents: An update. *Coord. Chem. Rev.* **2013**, *257* (19−20), 2689−2704.

(6) Estrada-Ortiz, N.; Guarra, F.; de Graaf, I. A. M.; Marchetti, L.; de Jager, M. H.; Groothuis, G. M. M.; Gabbiani, C.; Casini, A. Anticancer Gold N-Heterocyclic Carbene Complexes: A Comparative in vitro and ex vivo Study. *ChemMedChem* **2017**, *12* (17), 1429−1435.

(7) Pratesi, A.; Cirri, D.; Durovic, M. D.; Pillozzi, S.; Petroni, G.; Bugarcic, Z. D.; Messori, L. New gold carbene complexes as candidate anticancer agents. *BioMetals* **2016**, *29* (5), 905−911.

(8) Liu, W. K.; Gust, R. Update on metal N-heterocyclic carbene complexes as potential anti-tumor Metallodrugs. *Coord. Chem. Rev.* **2016**, *329*, 191−213.

(9) Zhang, X. N.; Selvaraju, K.; Saei, A. A.; D'Arcy, P.; Zubarev, R. A.; Arner, E. S. J.; Linder, S. Repurposing of auranofin: Thioredoxin reductase remains a primary target of the drug. *Biochimie* **2019**, *162*, 46−54.

(10) Mora, M.; Gimeno, M. C.; Visbal, R. Recent advances in gold-NHC complexes with biological properties. *Chem. Soc. Rev.* **2019**, *48*, 447−462.

(11) Mirzadeh, N.; Reddy, T. S.; Bhargava, S. K. Advances in diphosphine ligand-containing gold complexes as anticancer agents. *Coord. Chem. Rev.* **2019**, *388*, 343−359.

(12) Marmol, I.; Quero, J.; Rodriguez-Yoldi, M. J.; Cerrada, E. Gold as a possible alternative to platinum-based chemotherapy for colon cancer. *Cancers* **2019**, *11*, 780−816.

(13) Cerrada, E.; Fernández-Moreira, V.; Gimeno, M. C. Gold and platinum alkynyl complexes for biomedical applications. In *Advances in Organometallic Chemistry*; Pérez, P., Ed.; Elsevier, Academic Press: 2019; Vol. *71*, pp 227−258.

(14) Porchia, M.; Pellei, M.; Marinelli, M.; Tisato, F.; Del Bello, F.; Santini, C. New insights in Au-NHCs complexes as anticancer agents. *Eur. J. Med. Chem.* **2018**, *146*, 709−746.

(15) Hussaini, S. Y.; Haque, R. A.; Razali, M. R. Recent progress in silver(I)-, gold(I)/(III)- and palladium(II)-N-heterocyclic carbene complexes: A review towards biological perspectives. *J. Organomet. Chem.* **2019**, *882*, 96−111.

(16) Liang, X. X.; Luan, S. X.; Yin, Z. Q.; He, M.; He, C. L.; Yin, L. Z.; Zou, Y. F.; Yuan, Z. X.; Li, L. X.; Song, X.; Lv, C.; Zhang, W. Recent advances in the medical use of silver complex. *Eur. J. Med. Chem.* **2018**, *157*, 62−80.

(17) Johnson, N. A.; Southerland, M. R.; Youngs, W. J. Recent Developments in the Medicinal Applications of Silver-NHC Complexes and Imidazolium Salts. *Molecules* **2017**, *22* (8), 1263.

(18) Medici, S.; Peana, M.; Nurchi, V. M.; Lachowicz, J. I.; Crisponi, G.; Zoroddu, M. A. Noble metals in medicine: Latest advances. *Coord. Chem. Rev.* **2015**, *284*, 329−350.

(19) Banti, C. N.; Hadjikakou, S. K. Anti-proliferative and anti-tumor activity of silver(I) compounds. *Metallomics* **2013**, *5* (6), 569−596.

(20) Lin, J. C. Y.; Huang, R. T. W.; Lee, C. S.; Bhattacharyya, A.; Hwang, W. S.; Lin, I. J. B. Coinage Metal-N-Heterocyclic Carbene Complexes. *Chem. Rev.* **2009**, *109* (8), 3561−3598.

(21) Medici, S.; Peana, M.; Crisponi, G.; Nurchi, V. M.; Lachowicz, J. I.; Remelli, M.; Zoroddu, M. A. Silver coordination compounds: A new horizon in medicine. *Coord. Chem. Rev.* **2016**, *327-328*, 349−359.

(22) Liu, W. K.; Gust, R. Metal N-heterocyclic carbene complexes as potential antitumor metallodrugs. *Chem. Soc. Rev.* **2013**, *42* (2), 755−773.

(23) Hindi, K. M.; Panzner, M. J.; Tessier, C. A.; Cannon, C. L.; Youngs, W. J. The Medicinal Applications of Imidazolium Carbene-Metal Complexes. *Chem. Rev.* **2009**, *109* (8), 3859−3884.

(24) Kascatan-Nebioglu, A.; Panzner, M. J.; Tessier, C. A.; Cannon, C. L.; Youngs, W. J. N-Heterocyclic carbene-silver complexes: A new class of antibiotics. *Coord. Chem. Rev.* **2007**, *251* (5−6), 884−895.

(25) Mercs, L.; Albrecht, M. Beyond catalysis: N-heterocyclic carbene complexes as components for medicinal, luminescent, and functional materials applications. *Chem. Soc. Rev.* **2010**, *39* (6), 1903−1912.

(26) Patra, M.; Gasser, G.; Metzler-Nolte, N. Small organometallic compounds as antibacterial agents. *Dalton Trans.* **2012**, *41* (21), 6350−6358.

(27) Lansdown, A. B. G. A Pharmacological and Toxicological Profile of Silver as an Antimicrobial Agent in Medical Devices. *Adv. Pharmacol. Sci.* **2010**, *2010*, 910686.

(28) Klasen, H. J. Historical review of the use of silver in the treatment of burns. I. Early uses. *Burns* **2000**, *26* (2), 117.

(29) Fox, C. L., Jr. Silver Sulfadiazine. A New Topical Therapy for Pseudomonas in Burns: Therapy of Pseudomonas Infection in Burns. *Arch. Surg.* **1968**, *96* (2), 184−188.

(30) Melaiye, A.; Youngs, W. J. Silver and its application as an antimicrobial agent. *Expert Opin. Ther. Pat.* **2005**, *15* (2), 125−130.

(31) Fox, C. L.; Modak, S. M. Mechanism of Silver Sulfadiazine Action on Burn Wound Infections. *Antimicrob. Agents Chemother.* **1974**, *5* (6), 582−588.

(32) Zhang, S.; Du, C.; Wang, Z.; Han, X.; Zhang, K.; Liu, L. Reduced cytotoxicity of silver ions to mammalian cells at high concentration due to the formation of silver chloride. *Toxicol. In Vitro* **2013**, *27* (2), 739.

(33) Pellei, M.; Gandin, V.; Marinelli, M.; Orsetti, A.; Del Bello, F.; Santini, C.; Marzano, C. Novel triazolium based 11th group NHCs:

https://dx.doi.org/10.1021/acs.inorgchem.0c02922
Inorg. Chem. XXXX, XXX, XXX−XXX

synthesis, characterization and cellular response mechanisms. *Dalton Trans.* **2015**, *44* (48), 21041.
(34) Banti, C. N.; Giannoulis, A. D.; Kourkoumelis, N.; Owczarzak, A. M.; Poyraz, M.; Kubicki, M.; Charalabopoulos, K.; Hadjikakou, S. K. Mixed ligand-silver(I) complexes with anti-inflammatory agents which can bind to lipoxygenase and calf-thymus DNA, modulating their function and inducing apoptosis. *Metallomics* **2012**, *4* (6), 545−560.
(35) Sanchez, O.; González, S.; Fernández, M.; Higuera-Padilla, A. R.; Leon, Y.; Coll, D.; Vidal, A.; Taylor, P.; Urdanibia, I.; Goite, M. C.; Castro, W. Novel silver(I) and gold(I)N-heterocyclic carbene complexes. Synthesis, characterization and evaluation of biological activity against tumor cells. *Inorg. Chim. Acta* **2015**, *437*, 143.
(36) Allison, S. J.; Sadiq, M.; Baronou, E.; Cooper, P. A.; Dunnill, C.; Georgopoulos, N. T.; Latif, A.; Shepherd, S.; Shnyder, S. D.; Stratford, I. J.; Wheelhouse, R. T.; Willans, C. E.; Phillips, R. M. Preclinical anti-cancer activity and multiple mechanisms of action of a cationic silver complex bearing N-heterocyclic carbene ligands. *Cancer Lett.* **2017**, *403*, 98.
(37) Eloy, L.; Jarrousse, A.-S.; Teyssot, M.-L.; Gautier, A.; Morel, L.; Jolivalt, C.; Cresteil, T.; Roland, S. Anticancer Activity of Silver-N-Heterocyclic Carbene Complexes: Caspase-Independent Induction of Apoptosis via Mitochondrial Apoptosis-Inducing Factor (AIF). *ChemMedChem* **2012**, *7* (5), 805−814.
(38) Hartinger, C. G.; Dyson, P. J. Bioorganometallic chemistry from teaching paradigms to medicinal applications. *Chem. Soc. Rev.* **2009**, *38* (2), 391.
(39) Visbal, R.; Fernández-Moreira, V.; Marzo, I.; Laguna, A.; Gimeno, M. C. Cytotoxicity and biodistribution studies of luminescent Au(I) and Ag(I) N-heterocyclic carbenes. Searching for new biological targets. *Dalton Trans.* **2016**, *45*, 15026−15033.
(40) Fourie, E.; Erasmus, E.; Swarts, J. C.; Tuchscherer, A.; Jakob, A.; Lang, H.; Joone, G. K.; Van Rensburg, C. E. J. Cytotoxicity of Hydrophylic Silver Carboxylato Complexes. *Anticancer Res.* **2012**, *32* (2), 519−522.
(41) Liu, J. J.; Galettis, P.; Farr, A.; Maharaj, L.; Samarasinha, H.; McGechan, A. C.; Baguley, B. C.; Bowen, R. J.; Berners-Price, S. J.; McKeage, M. J. In vitro antitumour and hepatotoxicity profiles of Au(I) and Ag(I) bidentate pyridyl phosphine complexes and relationships to cellular uptake. *J. Inorg. Biochem.* **2008**, *102* (2), 303.
(42) Santini, C.; Pellei, M.; Papini, G.; Morresi, B.; Galassi, R.; Ricci, S.; Tisato, F.; Porchia, M.; Rigobello, M. P.; Gandin, V.; Marzano, C. In vitro antitumour activity of water soluble Cu(I), Ag(I) and Au(I) complexes supported by hydrophilic alkyl phosphine ligands. *J. Inorg. Biochem.* **2011**, *105* (2), 232.
(43) Abbehausen, C.; Heinrich, T. A.; Abrao, E. P.; Costa-Neto, C. M.; Lustri, W. R.; Formiga, A. L. B.; Corbi, P. P. Chemical, spectroscopic characterization, DFT studies and initial pharmacological assays of a silver(I) complex with N-acetyl-L-cysteine. *Polyhedron* **2011**, *30* (4), 579−583.
(44) Cardoso, J. M. S.; Correia, I.; Galvao, A. M.; Marques, F.; Carvalho, M. F. N. N. Synthesis of Ag(I) camphor sulphonylimine complexes and assessment of their cytotoxic properties against cisplatin-resistant A2780cisR and A2780 cell lines. *J. Inorg. Biochem.* **2017**, *166*, 55−63.
(45) Ortego, L.; Meireles, M.; Kasper, C.; Laguna, A.; Villacampa, M. D.; Gimeno, M. C. Group 11 complexes with amino acid derivatives: Synthesis and antitumoral studies. *J. Inorg. Biochem.* **2016**, *156*, 133−144.
(46) Zachariadis, P. C.; Hadjikakou, S. K.; Hadjiliadis, N.; Skoulika, S.; Michaelides, A.; Balzarini, J.; De Clercq, E. Synthesis, Characterization and in Vitro Study of the Cytostatic and Antiviral Activity of New Polymeric Silver(I) Complexes with Ribbon Structures Derived from the Conjugated Heterocyclic Thioamide 2-Mercapto-3,4,5,6-tetra- hydropyrimidine. *Eur. J. Inorg. Chem.* **2004**, *2004* (7), 1420−1426.
(47) Ciol, M. R.; Manzano, C. M.; Cuin, A.; Pavan, F. R.; Ribeiro, C. M.; Ruiz, A. L. T. G.; de Oliveira, E. C. S.; Lustri, W. R.; Fregonezi, N. F.; Nogueira, F. A. R.; Corbi, P. P. A Silver Complex with Cycloserine: Synthesis, Spectroscopic Characterization, Crystal Structure and In Vitro Biological Studies. *ChemistrySelect* **2018**, *3* (6), 1719−1726.
(48) Salvador-Gil, D.; Ortego, L.; Herrera, R. P.; Marzo, I.; Gimeno, M. C. Highly active group 11 metal complexes with α-hydrazidophosphonate ligands. *Dalton Trans.* **2017**, *46*, 13745−13755.
(49) Zaky, R. R.; Abdelghay, A. M. Synthesis, characterization and anticancerous properties of mixed ligand Pd(II) and Ag(I) complexes with 2-amino-7-oxo-4,5,6,7-tetrahydrobenzo[b]thiophene-3-carbonitrile and 2,2′-bipyridyl. *Res. J. Pharmaceut. Biol. Chem. Sci.* **2011**, *2* (1), 757−764.
(50) Poyraz, M.; Banti, C. N.; Kourkoumelis, N.; Dokorou, V.; Manos, M. J.; Simčič, M.; Golič-Grdadolnik, S.; Mavromoustakos, T.; Giannoulis, A. D.; Verginadis, I. I.; Charalabopoulos, K.; Hadjikakou, S. K. Synthesis, structural characterization and biological studies of novel mixed ligand Ag(I) complexes with triphenylphosphine and aspirin or salicylic acid. *Inorg. Chim. Acta* **2011**, *375* (1), 114−121.
(51) Li, D.-D.; Fang, F.; Li, J.-R.; Du, Q.-R.; Sun, J.; Gong, H.-B.; Zhu, H.-L. Discovery of 6-substituted 4-anilinoquinazolines with dioxygenated rings as novel EGFR tyrosine kinase inhibitors. *Bioorg. Med. Chem. Lett.* **2012**, *22* (18), 5870−5875.
(52) Zhang, D.; Yan, Y.; Jin, G.; Liu, B.; Ma, X.; Han, D.; Jia, X. Synthesis and antitumor evaluation of novel 4-anilino-7,8-dihydropyrido[4,3-d]pyrimidine-6(5H)-carboxylate derivatives as potential EGFR inhibitors. *Arch. Pharm.* **2018**, *351* (9), 1800110.
(53) Mabkhot, Y. N.; Alatibi, F.; El-Sayed, N. N. E.; Al-Showiman, S.; Kheder, N. A.; Wadood, A.; Rauf, A.; Bawazeer, S.; Hadda, T. B. Antimicrobial Activity of Some Novel Armed Thiophene Derivatives and Petra/Osiris/Molinspiration (POM) Analyses. *Molecules* **2016**, *21*, 222.
(54) Gramec, D.; Peterlin Mašič, L.; Sollner Dolenc, M. Bioactivation Potential of Thiophene-Containing Drugs. *Chem. Res. Toxicol.* **2014**, *27* (8), 1344−1358.
(55) Lawrance, G. A. Coordinated trifluoromethanesulfonate and fluorosulfate. *Chem. Rev.* **1986**, *86* (1), 17−33.
(56) van Geelen, C. M. M.; de Vries, E. G. E.; Le, T. K. P.; van Weeghel, R. P.; de Jong, S. Differential modulation of the TRAIL receptors and the CD95 receptor in colon carcinoma cell lines. *Br. J. Cancer* **2003**, *89* (2), 363−373.
(57) Tolan, D.; Gandin, V.; Morrison, L.; El-Nahas, A.; Marzano, C.; Montagner, D.; Erxleben, A. Oxidative Stress Induced by Pt(IV) Prodrugs Based on the Cisplatin Scaffold and Indole Carboxylic Acids in Axial Position. *Sci. Rep.* **2016**, *6*, 29367.
(58) Marmol, I.; Castellnou, P.; Alvarez, R.; Gimeno, M. C.; Rodriguez-Yoldi, M. J.; Cerrada, E. Alkynyl Gold(I) complexes derived from 3-hydroxyflavones as multi-targeted drugs against colon cancer. *Eur. J. Med. Chem.* **2019**, *183*, 111661.
(59) Marmol, I.; Virumbrales-Munoz, M.; Quero, J.; Sanchez-De-Diego, C.; Fernandez, L.; Ochoa, I.; Cerrada, E.; Yoldi, M. J. R. Alkynyl gold(I) complex triggers necroptosis via ROS generation in colorectal carcinoma cells. *J. Inorg. Biochem.* **2017**, *176*, 123−133.
(60) Gonzalez-Barcia, L. M.; Fernandez-Farina, S.; Rodriguez-Silva, L.; Bermejo, M. R.; Gonzalez-Noya, A. M.; Pedrido, R. Comparative study of the antitumoral activity of phosphine-thiosemicarbazone gold(I) complexes obtained by different methodologies. *J. Inorg. Biochem.* **2020**, *203*, 110931.
(61) Liu, X. H.; Rose, D. P. Differential expression and regulation of cyclooxygenase-1 and −2 in two human breast cancer cell lines. *Cancer Res.* **1996**, *56* (22), 5125−5127.
(62) Sambuy, Y.; De Angelis, I.; Ranaldi, G.; Scarino, M. L.; Stammati, A.; Zucco, F. The Caco-2 cell line as a model of the intestinal barrier: influence of cell and culture-related factors on Caco-2 cell functional characteristics. *Cell Biol. Toxicol.* **2005**, *21* (1), 1−26.
(63) Badisa, R. B.; Darling-Reed, S. F.; Joseph, P.; Cooperwood, J. S.; Latinwo, L. M.; Goodman, C. B. Selective Cytotoxic Activities of Two Novel Synthetic Drugs on Human Breast Carcinoma MCF-7 Cells. *Anticancer Res.* **2009**, *29* (8), 2993−2996.

https://dx.doi.org/10.1021/acs.inorgchem.0c02922
Inorg. Chem. XXXX, XXX, XXX−XXX

(64) Xu, X. B.; Lai, Y. Y.; Hua, Z. C. Apoptosis and apoptotic body: disease message and therapeutic target potentials. *Biosci. Rep.* **2019**, *39*, BSR20180992.
(65) Saraste, A.; Pulkki, K. Morphologic and biochemical hallmarks of apoptosis. *Cardiovasc. Res.* **2000**, *45* (3), 528−537.
(66) Park, S. J.; Kim, I. S. The role of p38 MAPK activation in auranofin-induced apoptosis of human promyelocytic leukaemia HL-60 cells. *Br. J. Pharmacol.* **2005**, *146* (4), 506−513.
(67) Park, N.; Chun, Y. J. Auranofin Promotes Mitochondrial Apoptosis by Inducing Annexin A5 Expression and Translocation in Human Prostate Cancer Cells. *J. Toxicol. Environ. Health, Part A* **2014**, *77* (22−24), 1467−1476.
(68) Redza-Dutordoir, M.; Averill-Bates, D. A. Activation of apoptosis signalling pathways by reactive oxygen species. *Biochim. Biophys. Acta, Mol. Cell Res.* **2016**, *1863* (12), 2977−2992.
(69) Aubrey, B. J.; Kelly, G. L.; Janic, A.; Herold, M. J.; Strasser, A. How does p53 induce apoptosis and how does this relate to p53-mediated tumour suppression? *Cell. Death. Differ.* **2018**, *25* (1), 104−113.
(70) Chen, J. D. The Cell-Cycle Arrest and Apoptotic Functions of p53 in Tumor Initiation and Progression. *Cold Spring Harbor Perspect. Med.* **2016**, *6* (3), a026104.
(71) Moloney, J. N.; Cotter, T. G. ROS signalling in the biology of cancer. *Semin. Cell Dev. Biol.* **2018**, *80*, 50−64.
(72) Ivanova, D.; Zhelev, Z.; Semkova, S.; Aoki, I.; Bakalova, R. Resveratrol Modulates the Redox-status and Cytotoxicity of Anticancer Drugs by Sensitizing Leukemic Lymphocytes and Protecting Normal Lymphocytes. *Anticancer Res.* **2019**, *39* (7), 3745−3755.
(73) Eloy, L.; Jarrousse, A. S.; Teyssot, M. L.; Gautier, A.; Morel, L.; Jolivalt, C.; Cresteil, T.; Roland, S. Anticancer Activity of Silver-N-Heterocyclic Carbene Complexes: Caspase-Independent Induction of Apoptosis via Mitochondrial Apoptosis-Inducing Factor (AIF). *ChemMedChem* **2012**, *7* (5), 805−814.
(74) Allison, S. J.; Sadiq, M.; Baronou, E.; Cooper, P. A.; Dunnill, C.; Georgopoulos, N. T.; Latif, A.; Shepherd, S.; Shnyder, S. D.; Stratford, I. J.; Wheelhouse, R. T.; Willans, C. E.; Phillips, R. M. Preclinical anti-cancer activity and multiple mechanisms of action of a cationic silver complex bearing N-heterocyclic carbene ligands. *Cancer Lett.* **2017**, *403*, 98−107.
(75) Zhu, Z. L.; Du, S. S.; Du, Y. B.; Ren, J.; Ying, G. G.; Yan, Z. Glutathione reductase mediates drug resistance in glioblastoma cells by regulating redox homeostasis. *J. Neurochem.* **2018**, *144* (1), 93−104.
(76) Quero, J.; Cabello, S.; Fuertes, T.; Marmol, I.; Laplaza, R.; Polo, V.; Gimeno, M. C.; Rodriguez-Yoldi, M. J.; Cerrada, E. Proteasome versus Thioredoxin Reductase Competition as Possible Biological Targets in Antitumor Mixed Thiolate-Dithiocarbamate Gold(III) Complexes. *Inorg. Chem.* **2018**, *57* (17), 10832−10845.
(77) Zhang, X.; Frezza, M.; Milacic, V.; Ronconi, L.; Fan, Y. H.; Bi, C. F.; Fregona, D.; Dou, Q. P. Inhibition of Tumor Proteasome Activity by Gold-Dithiocarbamato Complexes via Both Redox-Dependent and -Independent Processes. *J. Cell. Biochem.* **2010**, *109* (1), 162.
(78) Alva, N.; Panisello-Rosello, A.; Flores, M.; Rosello-Catafau, J.; Carbonell, T. Ubiquitin-proteasome system and oxidative stress in liver transplantation. *World J. Gastroenterol.* **2018**, *24* (31), 3521−3530.
(79) Bardaji, M.; Crespo, O.; Laguna, A.; Fischer, A. K Structural characterization of silver(I) complexes $[Ag(O_3SCF_3)(L)]$ (L = PPh_3, PPh_2Me, SC_4H_8) and $[AgLn](CF_3SO_3)$ (n = 2−4), (L = PPh_3, PPh_2Me). *Inorg. Chim. Acta* **2000**, *304* (1), 7−16.
(80) Sanchez-de-Diego, C.; Marmol, I.; Perez, R.; Gascon, S.; Rodriguez-Yoldi, M. J.; Cerrada, E. The anticancer effect related to disturbances in redox balance on Caco-2 cells caused by an alkynyl gold(I) complex. *J. Inorg. Biochem.* **2017**, *166*, 108−121.

https://dx.doi.org/10.1021/acs.inorgchem.0c02922
Inorg. Chem. XXXX, XXX, XXX−XXX